PEG-PEPTIDE DRUG CARRIER SYSTEMS WITH ENZYMATIC DEGRADATION UNITS

Nesligül YÜKSEL

İzmir Institute of Technology

December, 2016

PEG-PEPTIDE DRUG CARRIER SYSTEMS WITH ENZYMATIC DEGRADATION UNITS

A Thesis Submitted to
the Graduate School of Engineering and Sciences of
Izmir Institute of Technology
in Partial Fulfillment of the Requirements for the Degree of

MASTER OF SCIENCE

in Chemical Engineering

by
Nesligül YÜKSEL

December 2016
IZMIR

We approve the thesis of **Nesligül YÜKSEL**

Examining Committee Members:

_____

Assist. Prof. Dr. Ayben TOP
Department of Chemical Engineering, Izmir Institute of Technology

_____

Prof. Dr. Seher Fehime ÇAKICIOĞLU ÖZKAN
Department of Chemical Engineering, Izmir Institute of Technology

_____

Assoc. Prof. Dr. Serap CESUR
Department of Chemical Engineering, Ege University

30 December 2016

_____

Assist. Prof. Dr. Ayben TOP
Supervisor, Department of Chemical Engineering
Izmir Institute of Technology

_____

Prof. Dr. Seher Fehime ÇAKICIOĞLU ÖZKAN
Head of the Department of Chemical Engineering

_____

Prof. Dr. Bilge KARAÇALI
Dean of the Graduate School of Engineering and Sciences

ACKNOWLEDGEMENTS

I would like to express my special thanks to my advisor, Assist. Prof. Dr. Ayben TOP, for her priceless advises invaluable experiences, continuous supervision and significant concern during my M.Sc. studies. It has been a great honor and privilege to work with her.

I would like to also thank to my committee members, Prof. Dr. Seher Fehime ÇAKICIOĞLU ÖZKAN and Assoc. Prof. Dr. Serap CESUR for their valuable suggestions and recommendations.

Prof. Dr. Talat Yalçın was indebted for kindly performing MALDI-TOF mass spectroscopy experiments at Biological Mass Spectrometry and Proteomics Facility located at the Chemistry Department. I am thankful to Prof. Dr. Mustafa M. DEMİR for making DLS experiments possible by giving an access to ZetaSizer instrument in his laboratory. I also appreciate to PhD student Gökhan TOPÇU from the Department of Material Science and Engineering, Research Specialist Deniz ŞİMŞEK from the Department of Chemical Engineering, Dr. Sedef TAMBURACI from the Department of Bioengineering and Research Specialist Mine BAHÇECİ from Centre for Materials Research for their helps in characterization steps.

I also want to thank to TUBİTAK (The Scientific and Technological Research Council of Turkey) for financial support. (3501 Career Project #112S554, PI= Assist. Prof. Ayben TOP)

I would like to thank especially to my colleagues, Beste BALCI, Efecan PAKKANER and MSc. student Canbike BAR for their help in the laboratory. My greatest gratitude goes to Ruti Ruth POLİTİ for her help and support for every step of this thesis.

Finally, I want to thank specially to my family; Hamiyet YÜKSEL and Can ŞENTÜRK, for their motivation and encouragement. Their support cannot be underestimated during my M.Sc.

ABSTRACT

PEG-PEPTIDE DRUG CARRIER SYSTEMS WITH ENZYMATIC DEGRADATION UNITS

In this study, it was aimed to develop drug delivery systems with high drug release rate, capable of overcoming multidrug resistance of cancer cells. The first generation drug delivery system (DDS) denoted as mPEG-AT3-DOX was prepared by methoxy polyethylene glycol (mPEG) and peptide conjugation, and the model anticancer drug, DOX, was attached to the mPEG-peptide carrier system using stable amide linkage. mPEG was used to increase blood circulation time of the DDS. Designed peptide (AT3 = $CG_3H_6R_2ALALG_3E$) controls release of the drug via RRALAL sequence, which is a substrate for a lysosomal enzyme, cathepsin B, overexpressed in most of the tumor cells. pH responsive histidines and reactive amino acids (glutamic acid and cysteine) for drug and mPEG conjugations were also added to the peptide sequence. The peptide synthesized by using Fmoc chemistry was conjugated to mPEG-maleimide via Michael addition reaction. DOX was attached to the carboxylic acid group present in the carrier system (mPEG-AT3) via amide linkage. Mass spectroscopy and HPLC were used to assess the purity of the AT3 and mPEG-AT3. At pH 7.4, mPEG-AT3-DOX exhibited bimodal size (hydrodynamic diameter) distribution at about 15 and 30 nm independent of pH. % DOX release from mPEG-AT3-DOX was observed to be below 10 % at neutral pH and pH 5.0 in the absence of cathepsin B, and increased to 17 ± 2 % in the presence of cathepsin B. Complete degradation of AT3 peptide within three hours in the presence of cathepsin B suggests lower than expected DOX release is due to aggregation tendency of the DDS. Cytotoxicity of the conjugates was evaluated using the lung cancer (A549) and prostate cancer (PC3) cell lines. At the end of 24 hours the absolute IC_{50} values of free DOX and mPEG-AT3-DOX were obtained as 1.37 ± 0.05 and 1.33 ± 0.11 for the A549 cell line, 1.51 + 0.07 and 1.63 + 0.80 μg equivalent DOX / ml for the PC3 cell line, respectively. Considering, these results, the second generation DDS will be designed to have more pronounced pH sensitive property by increasing the number of histidines in the peptide domain.

ÖZET

ENZİMATİK BOZUNUR ÜNİTELİ PEG-PEPTİD İLAÇ TAŞIYICI SİSTEMLERİ

Bu çalışmada, kanser hücrelerinin çoklu ilaç direncinin çözümüne yönelik hızlı ilaç salım kabiliyetine sahip ilaç taşıyıcı sistemlerinin geliştirilmesi amaçlanmıştır. Birinci nesil ilaç taşıyıcı sistemi metoksi polietilen glikol ve peptid konjugasyonuyla hazırlanmış ve model kanser ilacı olan DOX, mPEG-peptid taşıyıcı sistemine kararlı amid bağı ile bağlanmıştır. İlaç taşıyıcı sisteminin kanda dolaşım süresini artırmak için mPEG kullanılmıştır. Tasarlanan peptid (AT3 = $CG_3H_6R_2ALALG_3E$) dizindeki RRALAL sayesinde bir çok kanserli hücrede aşırı üretilen lizozomal bir enzim olan katepsin B için substrat vazifesi görerek ilacın salınımı kontrol etmektedir. pH cevaplayabilen histidinler ile birlikte ilaç ve mPEG'in konjugasyonları için reaktif amino asitler de (glutamik asit ve sistein) peptid dizinine eklenmiştir. Fmoc kimyası uygulanarak sentezlenen peptidin mPEG-maleimid ile konjugasyonu Michael ekleme reaksiyonuyla gerçekleştirilmiştir. DOX ise taşıyıcı sistemde (mPEG-AT3) bulunan karboksilik asit gruplarına amid bağıyla bağlanmıştır. AT3 ve mPEG-AT3'ün saflığı kütle spektroskopisi ve HPLC kullanılarak belirlenmiştir. mPEG-AT3-DOX pH'tan bağımsız olarak yaklaşık 15 ve 30 nm'de ikili boyut (hidrodinamik çap) dağılımı göstermiştir. mPEG-AT3-DOX'un % DOX salımı nötral pH'da ve pH 5.0'te enzim kullanılmadığı zaman % 10'un altında; katepsin B varlığında ise % 17 ± 2'ye çıkmıştır. AT3 peptidinin katepsin B varlığında 3 saat içinde parçalanması, beklenenden az gerçekleşen DOX salımının ilaç taşıyıcı sisteminin kümelenme eğilimi dolayısıyla olduğunu önermektedir. Konjugatların sitotoksisitesi akciğer kanseri (A549) ve prostat kanseri (PC3) hücre hatları kullanılarak belirlenmiştir. 24 saat sonunda, serbest DOX ve mPEG-AT3-DOX'un mutlak IC_{50} değerleri A549 hücre hattı için sırasıyla 1.37 ± 0.05 ve 1.33 ± 0.11 ve PC3 hücre hattı için sırasıyla 1.51 ± 0.07 ve 1.63 ± 0.80 μg eşdeğer DOX/ml olarak elde edilmiştir. Bu sonuçları göze alarak ikinci nesil ilaç taşıyıcı sistemler peptid dizinine daha fazla histidin eklenerek pH'ya karşı daha duyarlı özellikte tasarlanacaktır.

TABLE OF CONTENTS

LIST OF FIGURES viii

LIST OF TABLES x

CHAPTER 1.INTRODUCTION 1

CHAPTER 2. LITERATURE REVIEW 6

2.1. Cancer Cells and Treatment Methods 6

2.2. Properties of Cancer Cells and Ideal Drug Delivery Systems 9

2.2.1. DDS Containing pH Sensitive Units 12

2.2.2. DDS Containing Enzymatically Degradable Units 14

CHAPTER 3. MATERIALS AND METHODS 19

3.1. Materials 19

3.2. Methods 20

3.2.1. Preparation of Methoxypolyethylene Glycol-Doxorubicin (mPEG-DOX) Conjugate 20

3.2.2. Preparation of mPEG-Peptide-DOX Conjugate 21

3.2.2.1. Solid Phase Peptide Synthesis 22

3.2.2.2. mPEG-Peptide Synthesis 22

3.2.2.3. mPEG-Peptide-DOX Synthesis 23

3.3. Characterization 24

3.3.1. Fourier Transform Infrared Spectroscopy (FTIR) Analysis 24

3.3.2. High Performance Liquid Chromatography (HPLC) 25

3.3.3. Mass Spectroscopy 26

3.3.4. UV Vis Spectroscopy 26

3.3.5. Size Measurement 27

3.3.6. Drug Release 28

3.3.7. Cytotoxicity Test 29

CHAPTER 4. RESULTS AND DISCUSSIONS.....33
4.1. Preparation of mPEG-DOX.....33
4.2. Preparation of mPEG-Peptide based DDS.....33
4.2.1. Peptide (AT3) Synthesis.....33
4.2.2. PEG-Peptide Conjugation.....34
4.3. Conjugation of DOX to mPEG-Peptide based DDS.....37
4.4. Characterization of DDS.....39
4.4.1. Size Measurement.....39
4.4.2. Drug Release Results.....44
4.4.3. Cytotoxicity Results.....46

CHAPTER 5. CONCLUSIONS.....53

REFERENCES.....55

APPENDIX A. SUPPLEMENTARY FIGURES.....60

LIST OF FIGURES

Figure **Page**

Figure 1. Proposed drug delivery system containing pH sensitive and enzymatically degradable units....4
Figure 2. Division behavior of normal cells and cancer cells.... 6
Figure 3. Stages of carcinogenesis 7
Figure 4. Schematic Representation of Metastasis Formation 8
Figure 5. Schematic representation of EPR effect 10
Figure 6. Illustration of MDR Effect....11
Figure 7. Adriamycin release from poly(histidine)-PEG and PLLA-PEG mixed micelles as a function of pH 13
Figure 8. DOX release kinetics of PEG-PH-PLLA at different pH values 14
Figure 9. Structure and drug release mechanism of pH-sensitive PLLA-poly(histidine)-PEG block copolymer based DDS 14
Figure 10. Cathepsin B and cystatin C activities in breast cancer 15
Figure 11. Comparison of cathepsin B activities in normal and tumor cells at different stages of colorectal cancer 16
Figure 12. HPLC curves of HSA-DOX taken at different incubation periods with cathepsin B at pH 5.0....17
Figure 13. Reaction scheme of mPEG-DOX conjugate.....21
Figure 14. Reaction scheme of preparation of mPEG-AT3 conjugate....23
Figure 15. mPEG-peptide-DOX conjugation reaction. 24
Figure 16. The acid hydrolysis reaction of DOX.....26
Figure 17. Expected morphology of PC3 30
Figure 18. Expected morphology of A549 30
Figure 19. Conversion of tetrazolium salts to formazan 32
Figure 20. MALDI-TOF MS spectrum of AT3 peptide.....34
Figure 21. HPLC Curves of (a) AT3, (b) mPEG-MAL and (c) mPEG-AT3. 35
Figure 22. MALDI-TOF Mass Spectrum of mPEG-AT3. 35
Figure 23. FTIR Spectra of (a) AT3, (b) mPEG-MAL and (c) mPEG-AT3. 36
Figure 24 HPLC curves of free DOX at 220 nm and 480 nm. 38
Figure 25 HPLC curves of mPEG-AT3-DOX at 220 nm and 480 nm 38

Figure 26. Size distributions of (a) AT3, (b) mPEG-MAL, and (c) mPEG-AT3. 39
Figure 27. Size distributions of mPEG-DOX measured at (a) 0 hr, (b) 24 hr, and (c) 48 hr.....40
Figure 28. Size distributions of mPEG-AT3-DOX measured at (a) 0 hr, (b) 24 hr, and (c) 48 hr. 41
Figure 29. AFM images of mPEG-DOX (a) 2-D image, (b) 3-D image, (c) particle size distribution, (d) absolute height distribution.....42
Figure 30. Two-dimensional AFM images of the PEG-AT3-DOX sample (a) diluted 5-times on the plate and (b) diluted 10-times and then added to the plate. 43
Figure 31. DOX release profile of mPEG-DOX and mPEG-AT3-DOX samples.....44
Figure 32. HPLC curves of AT3 peptide (a) before being treated with cathepsin B, (b) after being treated with cathepsin B for 3 hours.....45
Figure 33. Absorbance values of PC3 cell lines as a function of cells number used in MTT assay. 46
Figure 34. Absorbance values of A549 cell lines as a function of cells number used in MTT assay. 46
Figure 35. AT3 peptide, mPEG-maleimide, and mPEG-AT3 samples obtained after 24 hours using the PC3 cell line (C = 1.5 mg / ml).....48
Figure 36. AT3 peptide, mPEG-maleimide, and mPEG-AT3 samples obtained after 48 hours using the PC3 cell line (C = 1.5 mg / ml).....48
Figure 37. AT3 peptide, mPEG-maleimide, and mPEG-AT3 samples obtained after 24 hours using the A549 cell line (C = 0.75 mg / ml).....49
Figure 38. AT3 peptide, mPEG-maleimide, and mPEG-AT3 samples obtained after 48 hours using the A549 cell line (C = 0.75 mg / ml).....49
Figure 39. Growth inhibition curves of free DOX and the DOX-conjugated DDS obtained at the end of 24 hours using PC3 cell line. 51
Figure 40. Growth inhibition curves of free DOX and the DOX-conjugated DDS obtained at the end of 48 hours using PC3 cell line. 51
Figure 41. Growth inhibition curves of free DOX and the DOX-conjugated DDS obtained at the end of 24 hours using A549 cell line. 52
Figure 42. Growth inhibition curves of free DOX and the DOX-conjugated DDS obtained at the end of 48 hours using PC3 cell line. 52

LIST OF TABLES

Table **Page**

Table 1. Aggregation, drug release and cytotoxic properties of PEG-DOX conjugates containing enzymatically degradable sequences. 18

Table 2. DOX conjugation yield and percentage of carrier systems. 37

Table 3. Absolute IC_{50} values of free DOX and the DOX-conjugated DDS. 50

Table 4. Statistical comparison of absolute IC_{50} values of free DOX and the DDS. 50

CHAPTER 1

INTRODUCTION

According to the statistics given by World Health Organization (WHO) approximately 14 million new cancer cases and 8.2 million cancer related deaths were reported in 2012. Within the next two decades, annual cancer cases will be expected to rise from 14 million to 22 million although cancers have a high chance of cure if detected early and treated adequately by implementing evidence-based strategies for cancer prevention (http://www.who.int/mediacentre/factsheets/fs297/en/). After the diagnosis, one or combinations of the three treatment techniques; surgery, radiotherapy, and chemotherapy can be suggested depending on cancer type and stage. Although surgical treatment was considered as the primary method for the removal of large solid tumors, this procedure may trigger the development of metastatic (spreading) cancer and it is not feasible for undetectable and metastatic cancer. Besides, surgical and radiation therapy was reported to cure only 40 % of all cancer patients and the remaining 60 % die as a result of metastatic disease. Curative potential of chemotherapy for most of the cancer types is still under investigation but chemotherapy alone has major impact on the treatment of such metastatic diseases as germ cell tumors, haematological malignancies, and persistent trophoblastic disease as well as on the cure rate of female patients with choriocarcinoma. (Verweij et al.; 2000; Feng et al.; 2003; Ottevanger et al.; 2005). Additionally, post-surgery chemotherapy (adjuvant chemotherapy) was reported to increase the survival rate of the breast cancer patients. When combined with radiotherapy (concomitant chemoradiation therapy), chemotherapy also showed beneficial effects to radiotherapy by improving vascularization and oxygenation (Verweij et al.; 2000).

Although, the goal in chemotherapy is to kill only tumor cells using toxic drugs, the therapy it offers was overshadowed by its harmful effects to healthy tissues (especially bone marrow and the gastrointestinal tract mucosa) due to non-specific activity of the cytotoxic drugs. The common side effects of the anticancer drugs were reported as nausea, vomiting, fatigue, and hair loss, which reduce life quality of patients. In order to improve therapeutic potential of the chemotherapic drugs and minimize their side effects, the toxic drugs should be directed to tumor-site more

specifically (Chari 1998; Abou-Jawde et al., 2003; Liu et al., 2007; Wong et al., 2007). Thus, ideal drug delivery system for cancer therapy must be designed to satisfy the following requirements (Tong et al., 2007; Hu et al., 2016):

- should carry the drug without leakage and release the drug at effective dose with minimum toxic effect,
- should have high blood circulation time to reach tumor site,
- should accumulate in tumor cell specifically

Different architectures including polymer-drug conjugates, micelles, nanoparticles, nanogels, vesicles and dendrimer have been proposed as drug delivery systems. (Tong et al., 2007). Of these structures, nanoparticles were considered to be promising drug delivery vehicles for the toxic drugs by increasing the solubility of the hydrophobic drugs and targeting the tumor site specifically, due to their size, which facilitates their penetration to the tumor cell but not allows their exposure to the healthy cells. Moreover, decorating nanoparticles with tumor cell targeting ligands was reported to enhance the targeting efficiency. Nanoparticles based on biocompatible synthetic polymers, liposomes and natural biopolymers were reported to be efficient drug carrier candidates when decorated with ligands and/or PEGylated to enhance blood circulation rate (Brannon-Peppas and Blanchette 2004; Sunderland 2006; Kooijmans et al., 2016; Suk et al., 2016). However, in order to be an efficient carrier, the nanoparticle system should also release the drug in a programmed way, in addition to its successful internalization by the tumor cells.

Multi-drug resistance (MDR) is one of the major problems that affect the efficacy of the chemotherapy but rarely addressed in the development of chemotherapic drug carrier systems. MDR is detoxification of the tumor cell triggered mainly by the p-glycoproteins (P-gp), an efflux transporter that transfer drugs out of the tumor cells thereby lowering the drug concentration below the therapeutic limit (Simon 1999; Lee et al., 2005; Xu et al., 2006; Devalapally et al., 2007). The first approach to deal with the MDR can be blockage of P-gp activity by loading drug carrier system with MDR modulators or reverters along with the cytotoxic drug. However, this approach can be problematic since it may also block P-gp activity in healthy cells by reducing clearance of the drug (Lee et al., 2005). More feasible approach can be fast release of the drugs into tumor cell cytoplasm ensuring a concentration above which the drug exhibits cytotoxic activity. The pH gradient in the endocytic pathway, which starts with neutral cytoplasmic pH around 7.2, drops to 5.5-6 in endosomes, and ends up to 4.5-5 in

lysosomes, can be exploited to facilitate fast accumulation of the drugs by dissolution or collapse of the nanoparticles in acidic environment of these organelles (Lee et al., 2005).

Corroborating with this hypothesis, drug delivery systems, which contain pH sensitive domains were shown to exhibit significantly faster drug release at endosomal pH values (under acidic pH conditions) compared to physiological pH (Etrych et al., 2001; Chen et al., 2010). Additionally, it was reported that systems including enzymatically degradable groups also have high drug release rate in the presence of endosomal enzymes (Etrych et al., 2001).

The aim of this study is to develop nearly-ideal first-generation drug delivery systems. Carrier systems were prepared by methoxy polyethylene glycol (mPEG) and peptide conjugation. The model anticancer drug, doxorubicin, (DOX) was attached to the carrier systems via stable amide bond to obtain the final form of the DDS. Peptide-free mPEG-DOX system was also prepared as a control system to assess the role of peptide. In the synthesis of drug delivery systems, polymerization methods have been mostly employed. Although the reaction yield is high, the molecular weight and composition control is not easy. In this study, on the other hand, the molecules with already known molecular weight and composition were conjugated to provide molecular level control of the drug delivery system.

Proposed drug delivery system (mPEG-AT3-DOX) composed of mPEG, a *de novo* peptide denoted as AT3 containing pH responsive and enzymatic degradable units and DOX is given in Figure 1, FDA approved, non-immunogenic, non-antigenic and hydrophilic mPEG molecule was used to impart high blood circulation time to the drug delivery system. pH sensitive and enzymatic degradation units were incorporated to the peptide domain of the DDS to provide fast release of the drug in endosomal compartments of tumor cells (Figure 1). pH responsiveness of the peptide sequence in the DDS was imparted via hexa-histidine domain. The other specific hexa-peptide, arginine-arginine-alanine-leucine- alanine-leucine (RRALAL) in the sequence is the substrate of a lysosomal enzyme cathepsin B, which was reported to have high expression levels for certain cancer types. The peptide domain also has specific conjugation sites for doxorubicin and mPEG.

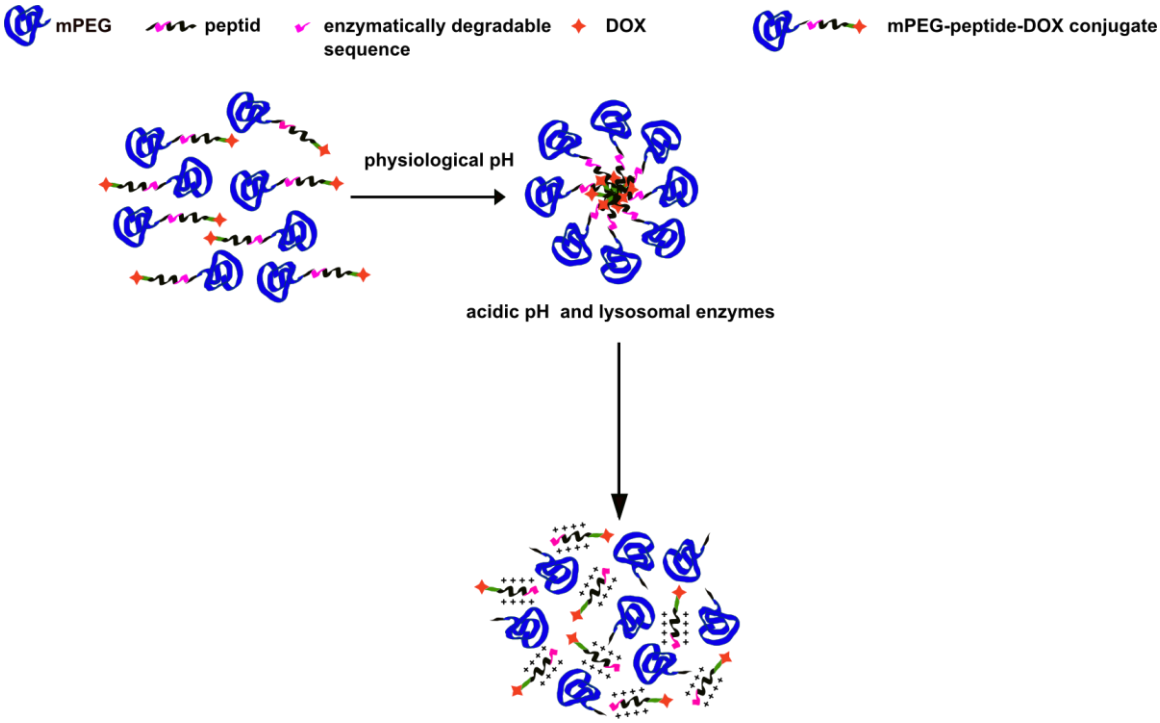

Figure 1. Proposed drug delivery system containing pH sensitive and enzymatically degradable units.

The purity and the functional groups of the carrier molecules were determined by spectroscopic and chromatographic methods. The size and stability of the drug delivery systems (mPEG-DOX and mPEG-AT3-DOX) were evaluated using dynamic light scattering (DLS). Atomic force microscopy (AFM) was employed to monitor morphology of the DDS. Drug release profiles of the DDS were determined in neutral and acidic buffer conditions and in the presence and absence of cathepsin B enzyme. Finally, the cytotoxicity of the DDS against A549 and PC3 cell lines was assessed using MTT assay.

This thesis includes 5 chapters; the first chapter is an introduction and the second chapter contains a literature review giving the state of art of the DDS used in cancer therapy. In the third chapter, materials and methods used to prepare and characterize the proposed DDS were explained. Results and discussion part is given in the fourth chapter. Finally, the fifth chapter concludes the thesis and gives suggestions and recommendations for the development of the next generation DDS. Although the reaction yield is high even though the molecular weight and composition control is not easy. In this study, the molecules which their molecular weight and composition are already known, was conjugated. Therefore, the reaction was controlled at the molecular level. In order to ensure a sustained high circulation time of the drug delivery system,

mPEG molecule was selected that is FDA approved, immunogenic, no antigenic and hydrophilic molecule. Peptides with pH sensitive and enzymatic degradation units were also mediate conjugation of doxorubicin and mPEG by adding to the sequence at the same time. In order to conjugate the drug to the carrier system, the stabile amide bond, which is degradable in the acidic medium, was used. pH responsiveness of the peptide sequence in the DDS was provided by hexa-histidine domain. Enzymatic degradability of the peptide was supported by tetra-peptide sequence, alanine-leucine- alanine-leucine (ALAL) sequences. The purity and the functional group of drug delivery systems and the constituent parts were determined by spectroscopic and chromatographic methods. The size of drug delivery systems was measured using dynamic light scattering (DLS) and atomic force microscopy (AFM). Drug release kinetics were studied in neutral, acidic and in containing endosomal enzyme cathepsin B acidic buffer solutions. Finally, the cytotoxicity of the conjugates was determined by the MTT test result using A549 and PC3 cell lines.

This thesis includes 5 chapters; the first chapter is an introduction, the second chapter describes the literature review, the third chapter explains material and methods, the fourth chapter discuss the results and the fifth chapter conclude the thesis and gives recommendations.

CHAPTER 2

LITERATURE REVIEW

This chapter explains the features of the cancer cells exploited in the development of drug delivery systems and the current status of drug delivery systems containing pH responsive and enzymatic degradation units.

2.1. Cancer Cells and Treatment Methods

Normally, cells divide only when the body needs them to replace aging or damaged cells whereas cancer cells exhibit an uncontrollable growth that causes the formation of a large mass of tissue, which is called tumor. Figure 2 shows these different division behaviors of the normal cells and the cancer cells. (http://rise.duke.edu/seek/pages/page.html?0205).

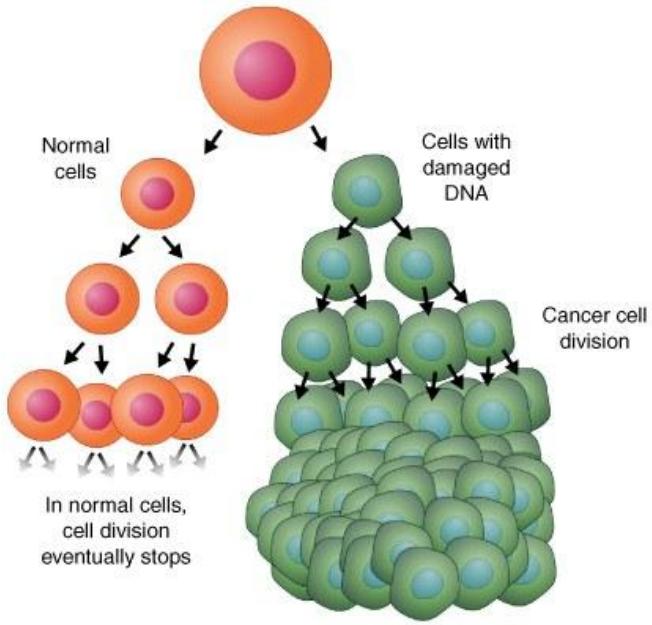

Figure 2. Division behavior of normal cells and cancer cells (Source: http://rise.duke.edu/seek/pages/page.html?0205).

Carcinogenesis, which is a transformation of normal cells to cancer cells, includes three main stages (Oliveira et al., 2007);

- ✓ Initiation stage

- ✓ Promotion stage
- ✓ Progression stage

As can be seen in Figure 3, in the initiation step, normal cells are underwent to mutation as a result of DNA damage by creating cells with adducts and this step is very fast. In the consecutive promotion stage, selective proliferation of initiated cells leads to the development of pre-neoplastic cells with changes in gene expression. During initiation and promotion, apoptosis and cell proliferation can occur at different rates, but in a balanced manner. In the progression stage, on the other hand, this balance is modified by accelerated cell growth without the presence of stimulate; eventually transforming preneoplastic lesions into malign lesions. This stage is irreversible and characterized by changes in the biochemical, metabolical and morphological characteristics of cells (Oliviera et al., 2007).

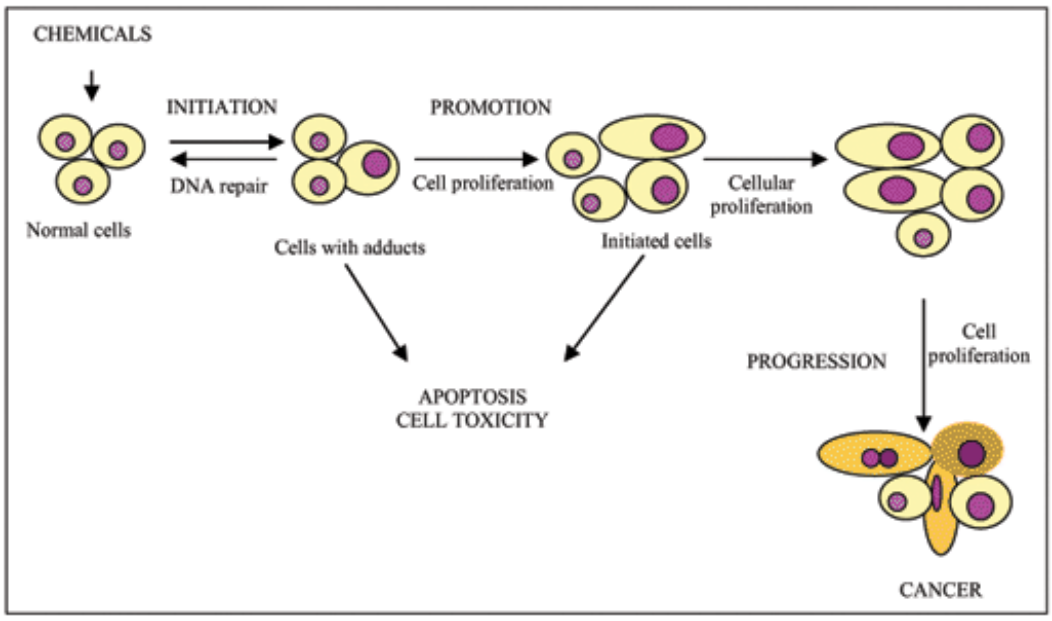

Figure 3. Stages of carcinogenesis
(Source: Oliviera et al., 2007).

At the initial stages of cancer, uncontrolled cell growth starts in a specific location called primary cancer site. However, some cancer cells have ability to penetrate the walls of lymphatic and/or blood cells where they can be transported to the other parts of the body. Spread of these specific cancer cells to nearby lymph nodes, tissues, or organs and distant parts of the body is called metastasis (Figure 4).

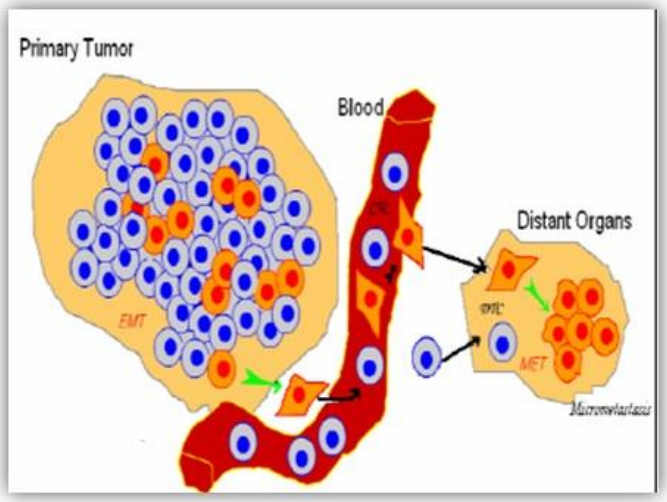

Figure 4. Schematic Representation of Metastasis Formation
(Source: http://www.viatarctcsolutions.com/technology/)

Three main treatment methods of cancer are chemotherapy, radiotherapy and surgery. The selection of the suitable treatment method depends on cancer type, size, location and patient's medical history and age. Radiation therapy uses high-energy particles or waves (usually X-rays) to control, kill or damage cancer cells. Surgical removal of tumor is applied when the tumor is large enough to manipulate. However, it is not proposed to use for all types of cancer such as, leukemia and lymphoma and during recovery stage, patients should take extreme precautions against infection risk (http://www.cancer.org/treatment/treatmentsandsideeffects/treatmenttypes/index). The third method, chemotherapy is the use of toxic drugs to kill the cancer cells. Cytotoxic medicines or drugs such as, doxorubicin, camptothecin, daunomycin and idarubicine are used in this technique to interfere DNA replication and cell division. It has major impact on the treatment of especially metastatic diseases. However there are lots of side effects of chemotherapy, as given below:

- ✓ Damage of healthy cells as well
- ✓ Hair loss
- ✓ Dry and sensitive skin
- ✓ Anorexia (vomiting) and weight loss
- ✓ Tiredness
- ✓ Infection risk because of the reduction of white blood cell

2.2. Properties of Cancer Cells and Ideal Drug Delivery Systems

In order to minimize the side effects and improve therapeutic potential of the chemotherapic drugs, a wide variety of drug delivery systems have been developed. These ideal drug delivery systems focus to target tumor tissues by avoiding normal cells. Additionally, they are designed to have high blood circulation time to arrive at tumor site without any leakage of the drug during transportation (Tong et al., 2007; Qin et al., 2016).

Enhanced permeability and retention (EPR) effect observed in cancer cells, has been widely exploited in the design of tumor-targeted drug delivery system. As it can be seen in Figure 5, pore size of the normal cell blood vessels is smaller than that of the cancer cells. Additionally, aberrant lymphatic drainage system of tumors cannot remove macromolecules and lipids from the interstitial space retaining these large molecules there over a longtime period. As a result of this abnormal pore structure of the cancer cells, small molecular weight free drugs can diffuse in cancer cell and leave from there easily. Nano-sized drug carriers, on the other hand, can penetrate into cancer cell and retain there. Hence, EPR effect gives macromolecular drugs a golden opportunity to access to tumor sites specifically by facilitating their accumulation inside the tumor cells at high concentrations. EPR effect can be observed with macromolecules with molecular weight greater than 40-50 kDa, even larger than 800 kDa, or of the size of bacteria and can be enhanced with increasing molecular weight of polymer as long as the size of the polymer fits pore size of tumor blood vessels (Maeda et al., 2001; Gabizon et al., 2004; Tong et al., 2007; Maeda et al., 2009; Liang et al., 2010; Bae et al., 2011; Maeda et al., 2012; Yuan et al., 2016). Chronologically, styrene-maleic acid copolymer-conjugated neocarzinostatin (SMANCS) first developed in 1979 eventually led to formulate the concept of the enhanced permeability and retention effect of solid tumors in 1986. Current examples of the molecules that utilize EPR effect are complex molecules such as micellar systems and liposomes containing anticancer drugs. Monoclonal antibody conjugates are other examples of such molecules with an increasing interest recently even though their limited success (Maeda et al., 2009). EPR-mediated accumulation was generally observed in all the tumor types where the highest percentage responses were reported for breast, lung and ovary tumors. However, poor

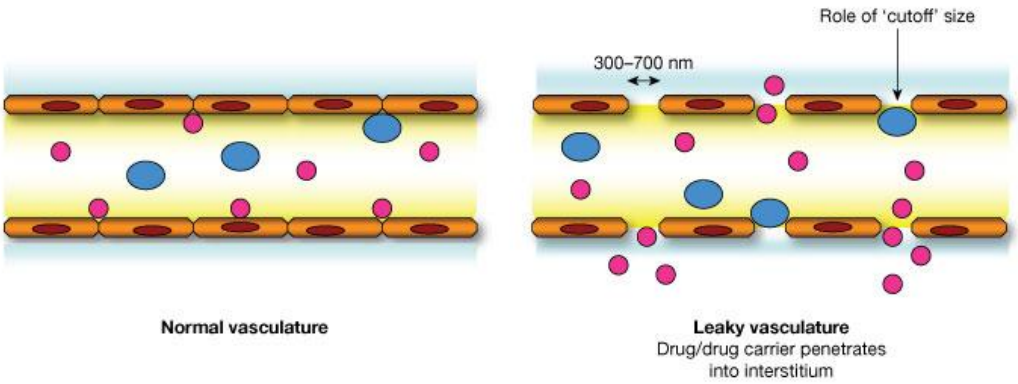

Figure 5. Schematic representation of EPR effect
(Source: https://www.intmedpress.com/journals/avcc/popup_fig.cfm?img=3e4c3ded-e20c-4d78-be99-a90b9c282720)

accumulation was obtained for colorectal, liver and pancreatic tumors due to their hypovascular properties (Rajora et al. 2014).

One of the challenges in the development of current drug delivery systems is to cope with multidrug resistance (MDR) effect which is a major factor in the failure of many forms of chemotherapy due to the development of resistance of cancer cell to chemotherapeutic drugs. Resistance to therapy has been correlated to the presence of molecular "pumps" in tumor-cell membranes that transports toxic drugs to the out of the cell before the drug exhibits its toxic properties within the nucleus or the cytoplasm (Figure 6). From ATP-binding cassette (ABC) membrane transporters three efflux-pumps, namely P-glycoprotein (Pgp-ABCB1), so-called multidrug resistance–associated protein-1 (MRP1/ABCC1)) and breast cancer resistant proteins 113 (ABCG2) were reported to commonly cause MDR effect. The relationship between P-glycoprotein and a drug-resistant phenotype were first discovered in Chinese hamster ovary cell lines in the mid-1970s. Studies on a lung cancer cell line resistant to doxorubicin and other chemotherapeutic agents which did not overexpress P-glycoprotein showed that another protein, MRP, expressed in this cell line is responsible for MDR effect (Persidis 1999; Saraswathy and Gong 2013). The cytotoxic drugs that are susceptible to MDR effect are hydrophobic or amphipathic chemotherapic agents, such as the taxanes (paclitaxel and docetaxel), vinca alkaloids

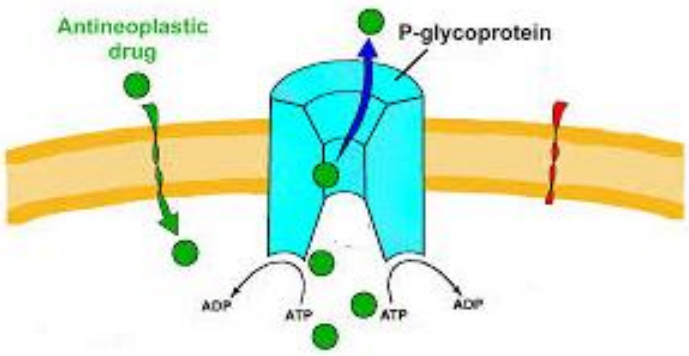

Figure 6. Illustration of MDR Effect
(Source: http://www.d.umn.edu/~jfitzake/Lectures/DMED/Antineoplastics/GeneralConcepts/MDR.html)

(vinorelbine, vincristine, and vinblastine), anthracyclines (doxorubicin, daunorubicin, and epirubicin), epipodophyllotoxins (etoposide and teniposide), antimetabolites (methorexate, fluorouracil, cytosar, 5-azacytosine, 6-mercaptopurine, and gemcitabine) topotecan, dactinomycin, and mitomycin C (Ozben 2006). One of the strategies to reverse the effect of MDR is the use of anticancer drugs that could escape from the ABC transporters such as alkylating drugs (cyclophosphamide), antimetabolites (5-fluorouracil), and the anthracycline modified drugs (annamycin and doxorubicin-peptide). The compounds so called MDR inhibitors, MDR modulators, MDR reversal agents or chemosensitizers, which are not inherently toxic but are able to inhibit ABC transporters, were also proposed. However, most of them failed in clinical trials by exhibiting low efficacy, high inherent toxicity or altering pharmacokinetics and biodistribution of anticancer drugs when co-administered with MDR inhibitors (Ozben 2006; Yin et al., 2013).

Nanoparticles which offer increasing therapeutic potential of anticancer agents due to their passive and active tumor targeting abilities, can potentially overcome MDR. They can bypass drug efflux by ABC transporters as they are internalized via either non-specific or specific endocytosis which results in a higher intracellular accumulation of the drug (Saraswathy and Gong 2013; Yuan et al., 2016). There exist reports demonstrating the reversal of MDR effect when DOX is attached to different nanoparticles including polyisobotylcyanuacrylate (PIBCA), polyisohexylcyanoacrylate (PIHCA), dextran and gold (Patel et al. 2013).

Although most nanoparticle DDS presented enhanced accumulation in tumor tissues, the poor cellular uptake and insufficient intracellular drug release remain rate-limiting steps for reaching the therapeutic drug concentration level. Thus, before quickly eliminated by the reversal cells, an ideal DDS should exhibit fast drug release to overcome MDR. Multifunctional stimuli-responsive delivery systems which ensure fast drug release kinetics by a change in pH, redox property or enzyme levels have been developed as alternative strategy for reversal of MDR (Yin et al. 2013).

2.2.1. DDS Containing pH Sensitive Units

pH-responsiveness is the most frequently used stimuli in the design of DDS. A typical pH-responsive DDS exhibits minimal anticancer drug release at physiological pH and unload the drugs through sensing pH descend in the interstitial space of solid tumors (pH 6.8–7.2) and intracellular endosomal compartments such as endosomes (pH 5–6) and lysosomes (pH 4.5–5.5) (Gillies et al., 2004; Yin et al. 2013).

Lee et al (2007) prepared pH-sensitive polymeric mixed micelles composed of poly(L-histidine) (polyHis; Mw 5000)/PEG (Mn 2000) and poly(L-lactic acid) (PLLA) (Mn 3000)/PEG (Mn 2000) block copolymers. While anticancer drug loaded micelle composed only PEG-polyhistidine delivery was relatively unstable at pH 7.4, incorporation of PLLA improved stability of the micellar structure at physiological pH. pH-dependent stability of the mixed micelles was monitored by relative light transmittance. Unexpectedly, the relative transmittance of the mixed micelles decreased with decreasing pH. This observation was explained by ionization of polyHis/PEG, followed by separation and isolation of PLLA/PEG from the micelles, which in turn formed more compact aggregates in water. Indeed, disintegration of the micelles by ionization of the imidazole group along polyHis chains was shown indirectly. Total amount of adriamycin release obtained at the end of 24 hrs of the mixed micelles as a function of release medium pH is given in Figure 7. The mixed micelles containing 25 wt.% PLLA/PEG (shown with closed triangles in Figure 7) released 32 wt.%, 70 wt.%, and 82 wt.% of ADR at pH 7.0, 6.8 and 5.0, respectively. It was also observed that increasing content of PLLA in the mixed micellar system suppressed the release of ADR. Thus, this study showed pH-dependent release of adriamycin tuned by the composition of the micelles.

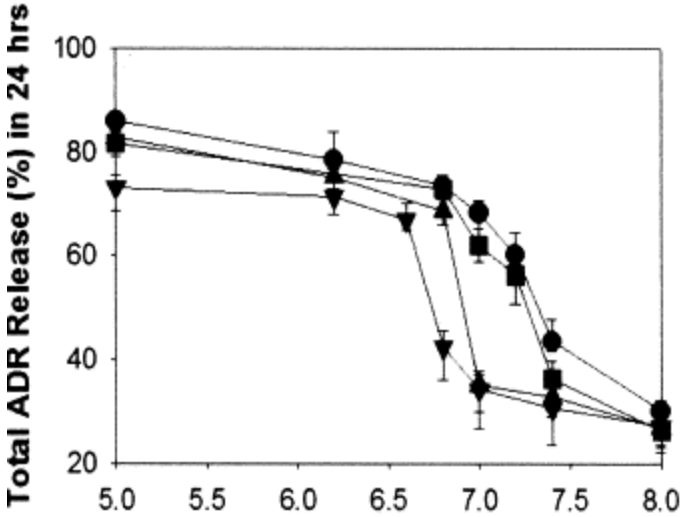

Figure 7. Adriamycin release from poly(histidine)-PEG and PLLA-PEG mixed micelles as a function of pH (Source: Lee et al., 2007).

In another study, pH sensitive drug carrier based on poly(ethylene glycol)-poly(L- histidine)-poly(L-lactide) PEG-PH-PLLA triblock copolymer were investigated. DOX release rate of this system was reported approximately 80% and less than 40% for pH 5.0 and pH 7.4 respectively at the end of 24 hrs clearly indicating its pH responsive behavior (Figure 8). Likewise the previous study, the pH responsiveness of the DDS was imparted by the poly(histidine) domain in the block copolymer. pK_a of the imidazole groups in histidine is approximately 6.0. At physiological pH, poly(histidine) block is neutral and PEG-PH-PLLA formed self-assembled nanoparticles (mean diameter of blank nanoparticles = ~140± 50 nm). However, when the pH value was lower than 6.0 the poly(histidine) block was protonized by partially destabilizing the micellar structure giving rise to increase the size of micelles (mean diameter of blank nanoparticles = ~180± 70 nm at pH 5.0) but making the micelles less compact thereby facilitating drug release as shown in Figure 9 (Liu et al., 2011).

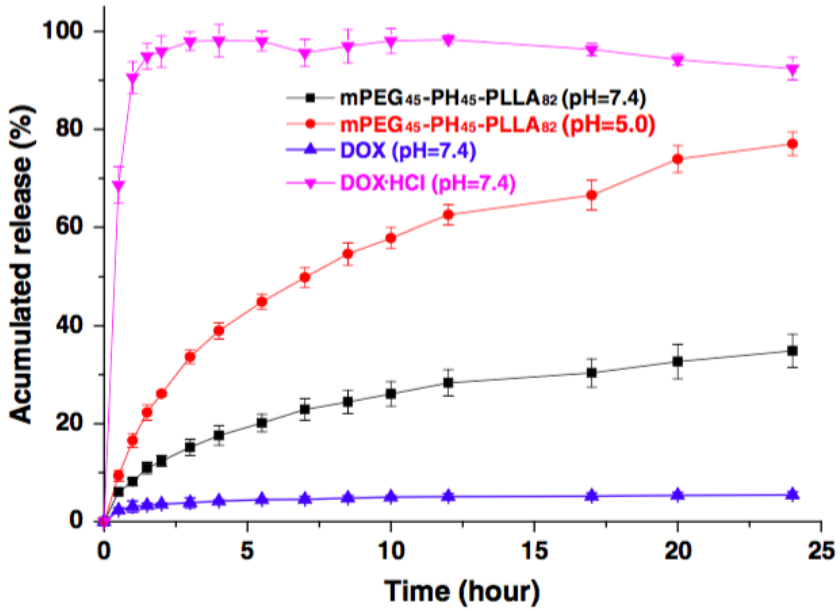

Figure 8. DOX release kinetics of PEG-PH-PLLA at different pH values (Source: Liu et al., 2011).

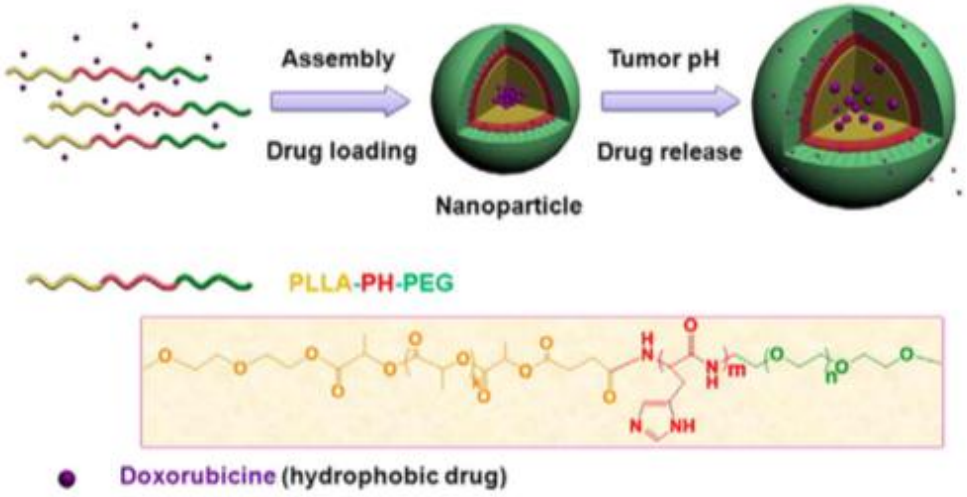

Figure 9. Structure and drug release mechanism of pH-sensitive PLLA-poly(histidine)-PEG block copolymer based DDS (Source: Liu et al., 2011).

2.2.2. DDS Containing Enzymatically Degradable Units

Cathepsin B, a lysosomal cysteine protease, is an important matrix protease frequently overexpressed in highly metastatic cancer cells. Indeed, it is the imbalance between cathepsin activity and cysteine proteinase inhibitors that causes invasion and metastasis in cancer cells as given in Figure 10 (Yano et al. 2001; Nomura and Katunuma 2005). Examples of cancer cells where cathepsin B is overexpressed

compared to normal tissues are coloracteral and breast cancer cell lines. As given in Figure 11, expression level of cathepsin B in coloracteral cancer cells is almost twice of that in normal cells (Doxakis et al., 2013). Similarly, expression ratios of cathepsin B to cystatin C mRNAs in human breast tissues determined by semiquantitative reverse transcriptase–polymerase chain reaction were found as 1.32 and 0.63 for cancer and normal tissue respectively (Yano et al. 2001). Thus, incorporation of lysosomal enzyme, especially cathepsin B, degradation sites into anticancer drug delivery systems may offer fast drug release in lysosomal compartments.

One of the earliest studies that is related to the test of a specific peptide sequence as a substrate for cathepsin B. For this purpose, Studer et al (1992) conjugated radiolabeled benzyl EDTA to an antibody via ALAL linker. Control conjugate system lacking ALAL sequence was also prepared. Incubation of these two conjugates in vitro with cathepsin B enzyme indicated that the conjugate with Ala-Leu-Ala-Leu was cleaved rapidly by the liver protease cathepsin B1 (half life = 6 h).

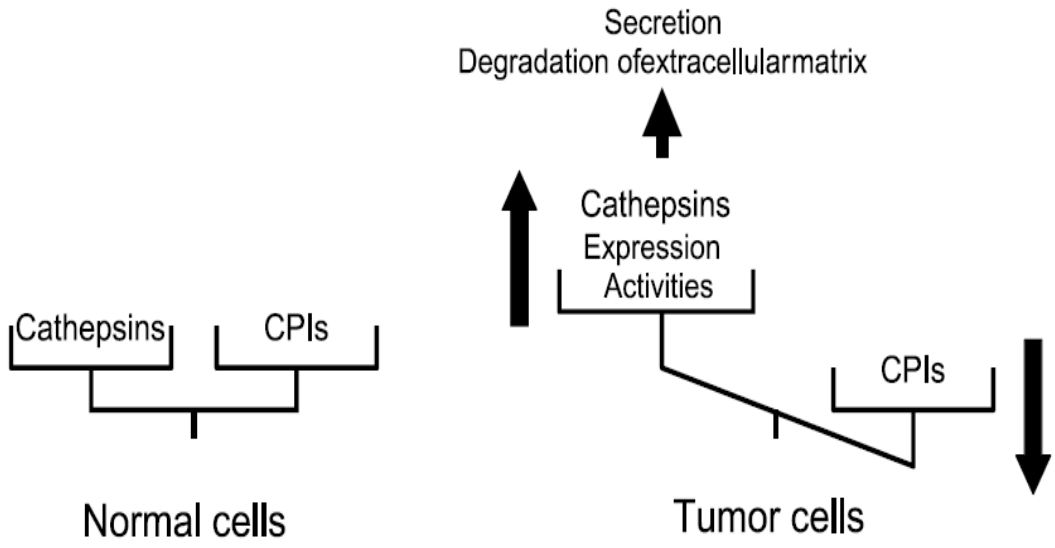

Figure 10. Cathepsin B and cystatin C activities in breast cancer
(Souce: Nomura and Katunuma 2005).

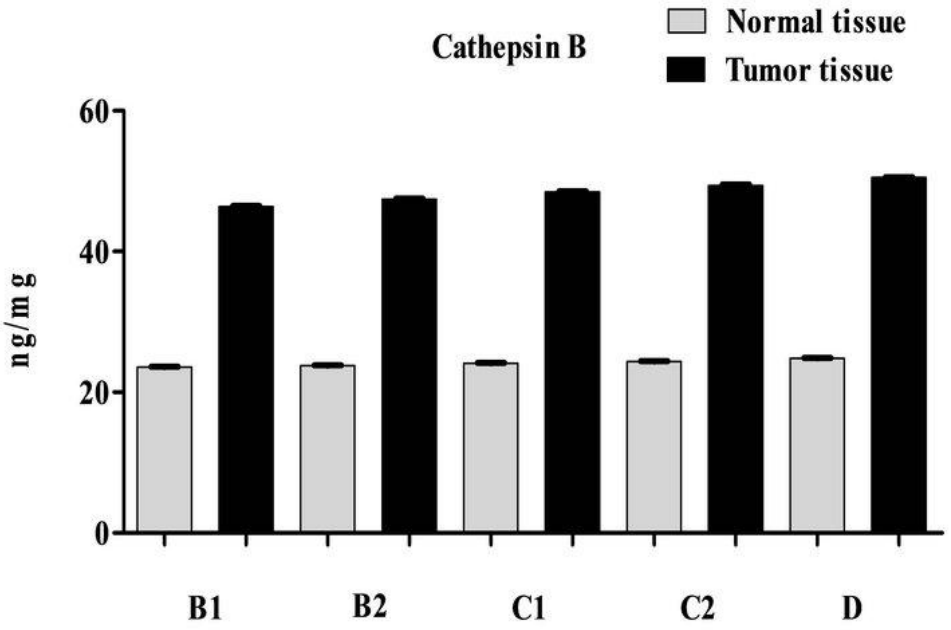

Figure 11. Comparison of cathepsin B activities in normal and tumor cells at different stages of colorectal cancer (Source: Doxakis et al., 2013).

In another study, Schmid et al (2007) designed a drug delivery system based on human serum albumin and anti-tumor drug, doxorubicin, conjugate containing enzymatically degradable linker RRALAL sequence. The drug conjugate was incubated with cathepsin B enzyme at pH 5.0 and the cleaved fractions were analyzed using HPLC periodically. It was shown that cathepsin B cleaved RRALAL sequence efficiently and very fast facilitating the release of DOX (Figure 12).

Veronesa et al. (2005) prepared a prodrug system based on PEG-peptide-DOX and investigated the effect of PEG architecture and structure and different enzymatically degradable peptide sequences on drug release and therapeutic activity. Aggregation, drug release and cytotoxic properties of these conjugates are summarized in Table 1. Of these conjugates PEG_{5000}-GFLG-DOX exhibited the highest aggregation number and release rate. It was reported that both GFLG and GLFG sequences were cleaved by the lysosomal enzymes and rate of DOX release was controlled by the peptidyl linker used but the nature of the PEG carrier had little influence on this process. Additionally, conjugates containing GFLG sequences showed superior cytotoxicity compared to those containing GLFG and GLG groups. In a similar study, DOX release was observed to be faster for HPMA based copolymers with GFLG linker compared to that lack of enzymatically degradable linker in the presence of cathepsin B (Etrych et al. 2001). Consequently, these studies clearly indicated that drug release properties of the carrier

systems could be controlled by the composition of the carrier molecule, pH sensitive and enzymatically degradable domains.

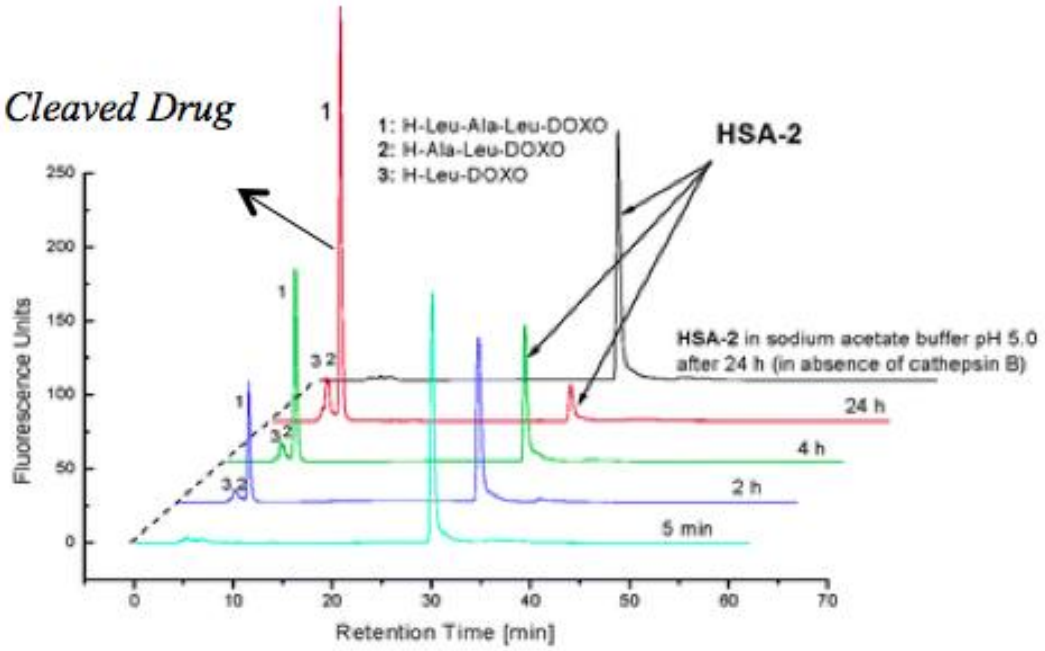

Figure 12. HPLC curves of HSA-DOX taken at different incubation periods with cathepsin B at pH 5.0 (Source: Schmid et al., 2007).

Table 1. Aggregation, drug release and cytotoxic properties of PEG-DOX conjugates containing enzymatically degradable sequences (Source: Veronesa et al. (2005).

Conjugate	**Structure**	**MW of PEG (Da)**	**Apparent MW (Da)**	**Aggregation Number**	**% release (24 hr)**	**IC50 (µg/ml)**
1	Linear PEG-GFLG-DOX	5000	120000	**20**	**75.9**	**5.2**
2	Branched PEG-GFLG-DOX	10000	33600	3	48.4	8.3
3	Linear PEG-GFLG-DOX	10000	33100	3	51.4	**4.6**
4	Branched PEG-GFLG-DOX	20000	N/A	N/A	60.6	6.7
5	Branched PEG-GLFG-DOX	10000	28400	2.6	**72.1**	**72**
6	Branched PEG-GLG-DOX	10000	30600	2.8	**37.6**	**105**

CHAPTER 3

MATERIALS AND METHODS

3.1. Materials

Methoxy polyethylene glycol-propionic acid (MW: 5000 g/mol with >80% COOH functionality), methoxypolyethylene glycol maleimide (MW:5000 g/mol with >90% maleimide functionality), (benzotriazol-1-yloxy)tripyrrolidinophosphonium hexafluorophosphate, 98% (PyBOP) and solvents, dimethyl sulfoxide (DMSO), and diethyl ether (DEE) were obtained from Sigma-Aldrich. N-ethyldiisopropylamine, 99% (DIPEA) and Doxorubicin HCI (DOX) were purchased from Alfa Aesar and Medkoo Biosciences respectively.

For solid phase peptide synthesis, rink amide MBHA resin, Fmoc-Cys-Trt-OH, Fmoc-Gly-OH, Fmoc-His-Trt-OH, Fmoc-Arg-(Pbf)-OH, Fmoc-Ala-OH, Fmoc-Leu-OH, Fmoc-Glu-(OtBu)-OH, (NovaBiochem), N,N,N,N-tetramethyl-O-(1H-benzotriazol-1-yl)uronium hexafluorophosphate (HBTU), 1-hydroxybenzotriazole hydrate (HOBt), (P3 Biosystems) dimethylformamide (DMF), dichloromethane (DCM), 4-methylmorpholine (NMM) (Sigma-Aldrich), and piperidine (Acros) were used. Triisopropyl silane (TIS), 1,3-dimethoxybenzene (DMB), and synthesis grade trifluoroacetic acid (TFA) (Merck) were employed in the preparation of cleavage cocktail.

Sodium chloride, sodium hydroxide, L-cysteine, ethylenediaminetetraacetic acid (EDTA) sodium salt (Sigma-Aldrich), sodium phosphate monobasic, imidazole (Fluka), sodium acetate, acetic acid and hydrochloric acid (Merck) were used to prepare the buffer solutions. Affinity chromatography and gel permeation chromatography were carried out using respective HisPur Ni-NTA (Thermo Scientific) and Sephadex LH-20 (GE Healthcare) resins. Snake skin (MW 3.5 kDa) dialysis tubing (Thermo Scientific) was used in dialysis process and drug release experiments. Merck cathepsin B (human liver, C = 0.53 mg protein/ml, specific activity >10 U/mg protein) was used in drug release experiments.

HPLC grade acetonitrile, 99.98% and spectroscopic grade TFA were purchased from Sigma-Aldrich and Merck, respectively. Sinapic acid (Sigma-Aldrich) and FTIR

grade potassium bromide (KBr) were employed in MALDI-TOF and FTIR spectroscopy analysis respectively.

European grade fetal bovine serum (FBS), gentamycin sulfate, trypsin.EDTA Solution C and 0.5% trypan blue solution were supplied from Biological Industries. Growth medium RPMI-1640 with L-glutamine and 3-(4,5-dimethylthiazol-2-yl)-2,5-diphenyltetrazolium bromide (MTT) were purchased from Sigma-Aldrich and Amresco, respectively. All the chemicals and solvents were used without purification.

3.2. Methods

3.2.1. Preparation of Methoxypolyethylene Glycol-Doxorubicin (mPEG-DOX) Conjugate

mPEG-DOX conjugate system was synthesized as a control system for the drug delivery system containing enzymatic degradation units incorporated its peptide domain. The model anticancer drug, doxorubicin, was attached to the polymeric carrier molecule, mPEG propionic acid using amine-carboxylic acid reaction via the formation of stable amide bond given in Figure 13. In a typical reaction, 20 mg mPEG (0.004 mmol) and 14.4 mg PyBOP (0.028 mmol) were dissolved in 4 ml DMSO and 9.6 µl DIPEA (0.055 µmol) and 8 mg DOX (0.0136 mmol) were added. The reaction was allowed to proceed in the dark at 30 °C and 120 rpm for 3 days. The reaction mixture, then, was precipitated on ice-cold (stored at -20 °C) diethyl ether to isolate mPEG-DOX conjugate. The precipitate (mainly mPEG-DOX conjugate) was washed with cold ether to remove some portion of unreacted DOX until no color was detected in washing solution. Residual DEE in the conjugate was evaporated in a fume hood. Dried pellet was dissolved in 2 ml DMSO and applied to gel permeation chromatography column containing Sephadex LH-20 resin suspended in DMSO to remove remaining unreacted DOX. Colorimetric PEG detection test based on the complex formation of barium iodide and PEG was applied to the fractions eluted from the column. In this method, approximately 4 µl of sample from elution fractions was diluted with 10 times excess of deionized water. Next, 10 µl of $BaCl_2$ (5% (w/v) barium chloride in 1 M HCl) solution and 5 µl of iodine (1.27 g iodine in 100 ml of 2% (w/v) KI) solution were added and the solution was vortexed.

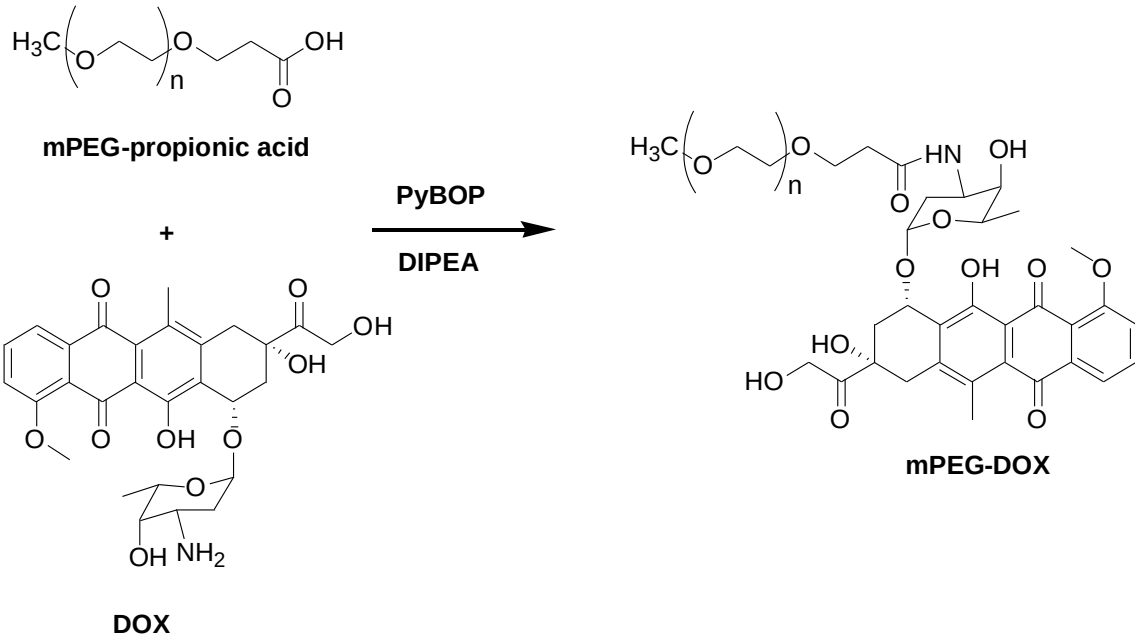

Figure 13. Reaction scheme of mPEG-DOX conjugate.

In this test, yellow color of the solution indicated PEG-free fractions and PEG containing fractions were identified by their brownish color (Gong et al., 2007). The collected fractions containing PEG corresponding to the isolated conjugate were precipitated on ice-cold DEE. After the removal of DEE in the fume hood, the conjugate was dissolved in deionized water; freeze dried and stored at -20 °C.

3.2.2. Preparation of mPEG-Peptide-DOX Conjugate

mPEG-Peptide-DOX conjugate system was synthesized using the following three steps:

- ✓ Solid phase peptide synthesis (SPPS)
- ✓ mPEG-Peptide conjugation
- ✓ Drug attachment

3.2.2.1. Solid Phase Peptide Synthesis

The peptide used in this study, denoted as AT3, with a sequence of $CG_3H_6R_2ALALG_3E$ was synthesized using AAPTEC Focus XI model automated peptide synthesis instrument. Solid phase peptide synthesis (SPPS) was conducted on a rink amide MBHA resin (0.66 mmol/g functionality) by employing Fmoc strategy at 0.1 mmol scale. Base-labile protecting groups of the resin and amino acids were removed by exposing to 20% piperidine in DMF for 15 min and the reaction was repeated three times. Carboxylic acid-amine conjugation reactions were carried out using the activating agents 0.395 mmol of HBTU dissolved in 3 ml DMF containing 0.4 mmol amino acid and 2.5 ml of 0.4 M NMM for 1 hr. In addition to these agents, 0.44 mmol HOBt was also used during the coupling of His and Cys residues to prevent racemization. For each amino acid double coupling cycles were performed. At the end of the synthesis, the resin was washed with DCM and dried under N_2 flow at room temperature. Cleavage reactions were conducted using 92.5:5:2.5 TFA:DMB:TIS cocktail (20 ml cocktail / g resin) for 2.5 hours. The resin was filtered using a polypropylene column and the supernatant was precipitated over cold DEE with 1:10 cleavage cocktail: DEE volume ratio. The precipitate was washed with DEE and centrifuged twice. After evaporation of DEE under N_2 flow at room temperature, the raw peptide was dissolved in 2 ml of 1% acetic acid in deionized water, freeze dried and stored at -20 ^{o}C.

3.2.2.2. mPEG-Peptide Synthesis

mPEG-maleimide (mPEG-MAL) was conjugated to thiol group of cysteine located at the N-terminal of the peptide via Michael addition reaction given in Figure 14. In this reaction, 40 mg (0.019 mmol) of peptide was dissolved in 5 ml of 0.1% acetic acid in deionized water, and solution pH was brought to a neutral pH by the addition of 15 ml of PBS buffer (100 mM of phosphate buffer with 150 mM of NaCl at pH 7.2) while passing nitrogen gas over the solution to avoid air oxidation of cysteines. Then, 100 mg (0.02 mmol) of PEG-MAL was added to the peptide solution under inert atmosphere and the solution was stirred at room temperature for 4 hours. Affinity chromatography based on the specific attraction forces between Ni-NTA resin and

histidines of the peptide and hence, mPEG-peptide conjugate was used to separate unreacted mPEG-MAL. In this technique, 50 mM phosphate buffer with 0.3 M NaCl at pH 8.0 was used as binding and washing buffer. After binding the histidine containing

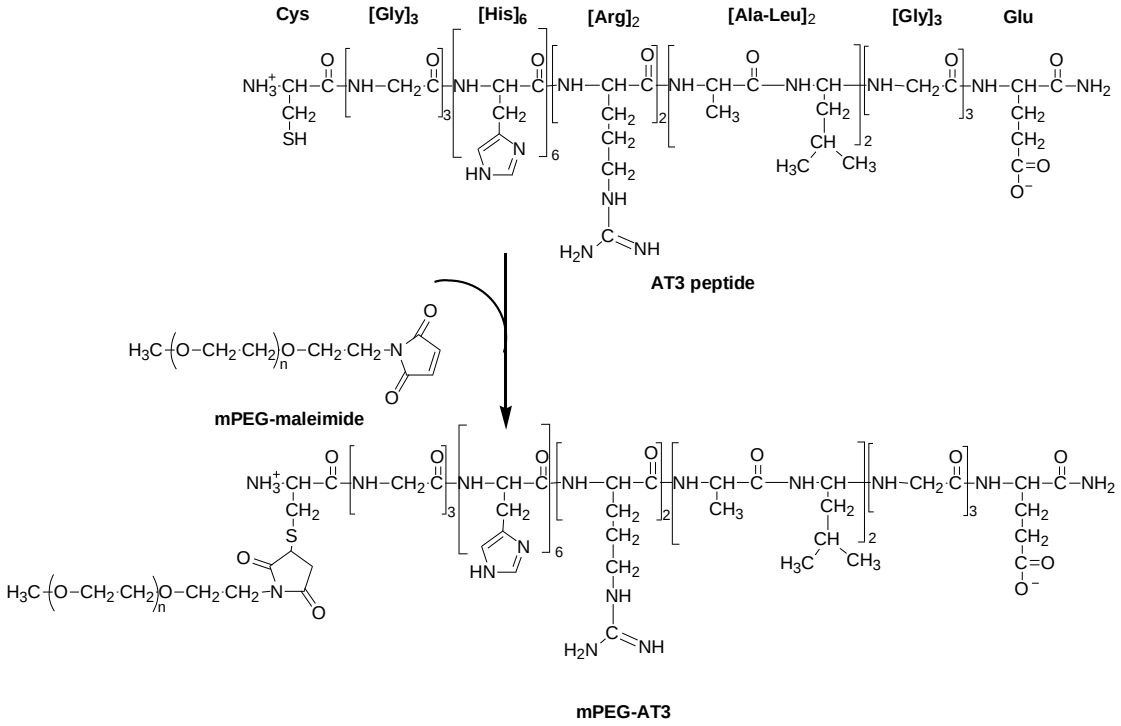

Figure 14. Reaction scheme of preparation of mPEG-AT3 conjugate.

species to the resin for overnight, the resin was washed until no PEG was detected in the solution after applying colorimetric assay. Elution of the peptide and mPEG-peptide was carried out using 50 mM phosphate containing 0.3 M NaCl and 0.5 M imidazole at pH 7.4. Then, unreacted peptide was removed by extensive dialysis against deionized water using a Snake skin dialysis tubing membrane (MWCO 3.5 kDa) until the conductivity of the solution in the membrane dropped below 10 μS/cm. At the end of the dialysis, the isolated mPEG-AT3 conjugate was freeze-dried and stored at -20 °C (yield = 16 ±1 %).

3.2.2.3. mPEG-Peptide-DOX Synthesis

Doxorubicin was attached to mPEG-AT3 with a reaction similar to mPEG-DOX conjugation. In this reaction amine group of DOX was attached to the carboxylic acid group of C-terminal glutamic acid in the peptide sequence via stable amide bond

conjugation (Figure 15). Approximately, 20 mg mPEG-peptide (0.004 mmol) and 14.4mg (0.028 mmol) PyBOP were dissolved in 4 ml DMSO and 9.6 µl DIPEA (0.055 µmol) and 8 mg DOX (0.0136 mmol) were added the reaction. The solution was stirred at 30 °C and 120 rpm.in dark for 3 days. To isolate mPEG-AT3-DOX, same procedure given in section 3.2.1 (mPEG-DOX synthesis) was applied.

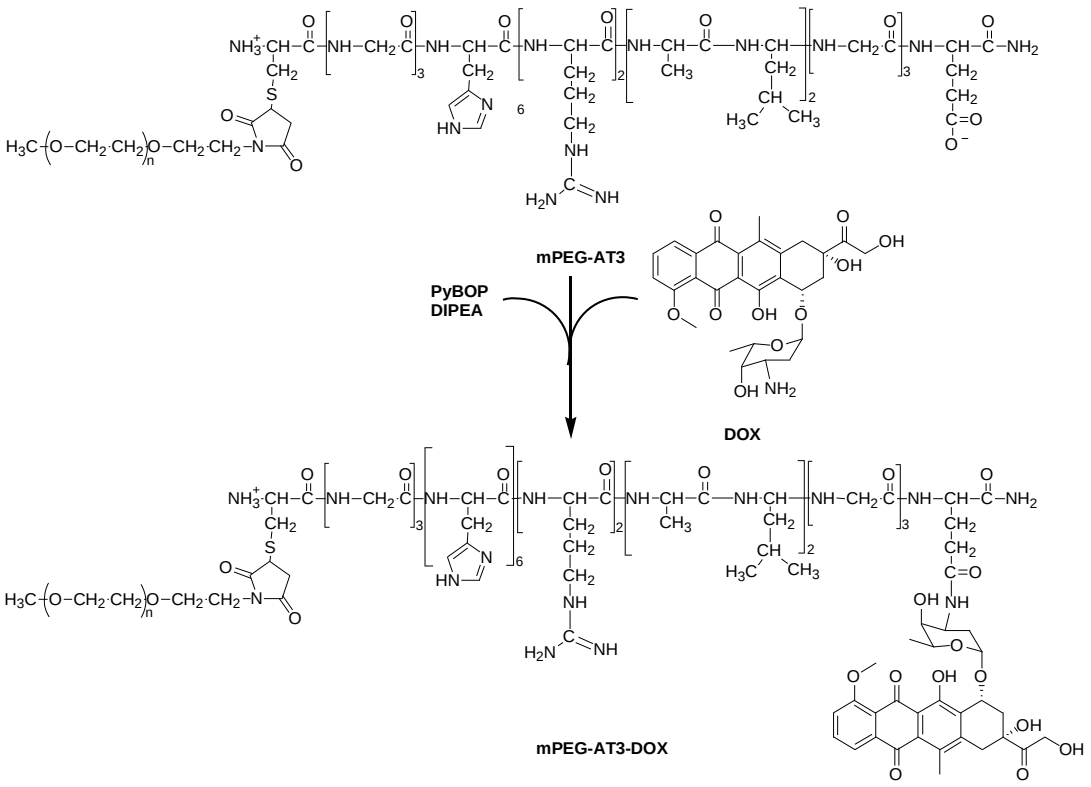

Figure 15. mPEG-peptide-DOX conjugation reaction.

3.3. Characterization

3.3.1. Fourier Transform Infrared Spectroscopy (FTIR) Analysis

Functional groups of mPEG-MAL, AT3 peptide, and mPEG-AT3 conjugate were determined by FTIR Spectroscopy on a Shimadzu IR Prestige-21 FTIR-8400S model spectrophotometer. Approximately 1 mg of sample demoisturized in a vacuum oven at room temperature and 150 mg of potassium bromide (KBr) were mixed and pulverized thoroughly to prepare a pellet, which was, then, inserted into sample holder to acquire spectrum. The range of wavenumbers was set between 400 and 4000 cm^{-1}.

3.3.2. High Performance Liquid Chromatography (HPLC)

Reverse phase HPLC method was used to assess purity of the samples and to monitor enzymatic cleavage reaction. For all runs, 0.1% TFA in deionized water and 0.08% TFA in acetonitrile were used as solvent A and solvent B respectively. In the analyses of AT3, mPEG-MAL and mPEG-AT3, the samples were dissolved in 0.1% TFA in deionized water (~1-2 mg/ml), filtered and 100 µl of sample was injected to C18 analytical column (Inertsil WP-300, 5µm, 4.6 x 100 mm). First, mixture of Solvent A and Solvent B at a ratio of 95:5 was passed through the column for 15 minutes. Then, Solvent A:Solvent B ratio was changed from 95:5 to 40:60 linearly within 40 minutes. Solvent flowrate was kept constant 1 ml/min and the elution profile of the samples was monitored at using a UV detector at 214 nm wavelength .

DOX and mPEG-AT3-DOX analyses were performed using a C18 column (Vydac 218TP54, 5µm, 4.6 x 250 mm) with 100 µl sample injection volume and at 0.8 ml / min flow rate. For these runs, Solvent A: Solvent B ratio was varied from 90:10 to 20:80 within 40 minutes. The chromatogram signals were acquired by using both 214 nm and 480 nm wavelengths.

To monitor cathepsin B activity, 1.5 mg of AT3 was dissolved in 1 ml of buffer (50 mM sodium acetate buffer with 150 mM NaCl, 1 mM EDTA, 5 mM L-cysteine at pH 5.0) and then, it was added to 10 µL of cathepsin B (0.53 mg / mL) after filtration. The solution was incubated at 37 °C for 3 hours, then 100 µl of solution injected into a C18 analytical column (Inertsil WP-300, 5 µm, 4.6 × 100 mm). Solvent A:Solvent B at a ratio of 95:5 was kept for 5 minutes and then, the ratio was changed to 40:60 in 50 minutes. During the analyses, solvent flowrate was set to 1 ml/min and a UV detector at 214 nm was used to monitor elution of the sample from the column. Additionally, HPLC chromatogram of the enzyme-free peptide was taken in the same conditions as a control sample. Agilent 1100 Model HPLC system was used in all reverse phase HPLC analyses.

3.3.3. Mass Spectroscopy

Mass spectroscopy of the samples was performed at Biological Mass Spectrometry and Proteomics Facility located at the Chemistry Department of İzmir Institute of Technology. Matrix-assisted laser desorption/ionization time of flight mass spectroscopy MALDI-TOF-MS (Bruker Daltonics – Autoflex III Smartbeam) was used to confirm MW of peptide and mPEG-peptide conjugate. The sample was dissolved in 0.1% TFA in deionized water and sinapic acid was utilized as matrix for the analyses.

3.3.4. UV Vis Spectroscopy

At high temperature, acid hydrolysis of DOX is resulted in cleavage of the glycosidic bond between aglycone (adriamycinone) and sugar (daunosamine) group as given in Figure 16. Thus, total DOX contents of the drug delivery systems containing stable amide bonds, mPEG-DOX and mPEG-AT3-DOX, were determined after liberating DOX as adriamycinone formed during acid hydrolysis reaction.

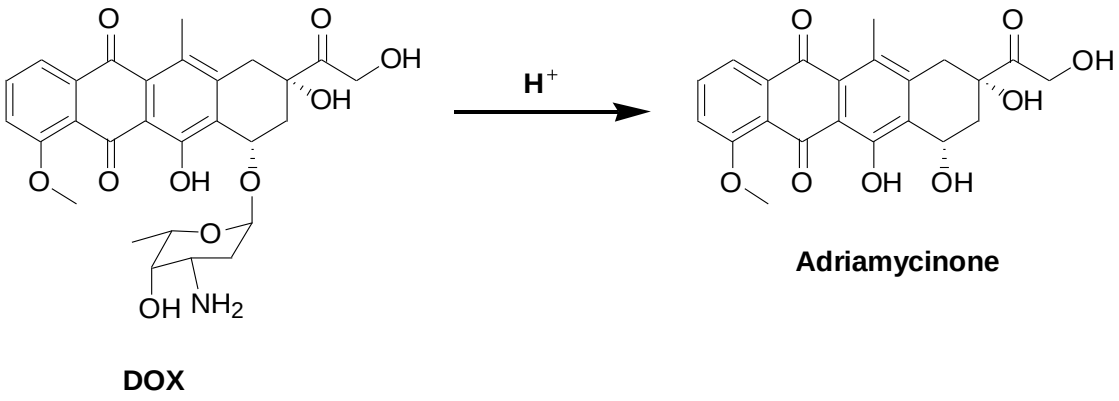

Figure 16. The acid hydrolysis reaction of DOX.

To prepare a calibration curve of adriamycinone, first, two stock solutions of DOX was prepared in DI water at ~40-50 µg/ml concentration range. Exact concentrations of the stock solutions were determined by measuring absorbance of DOX at 488 nm and using the molar absorption coefficient of DOX at this wavelength, 11500 $L \cdot mol^{-1} \cdot cm^{-1}$. 200 µl of the DOX stock solution was mixed with equal volume

of 2N HCl and the resultant solution was incubated at 50 °C for 2 hours. After the hydrolysis reaction, 1.2 ml of DMSO was added. Serial dilutions were prepared by using 1:3 volume ratio of 1N HCl: DMSO and absorbance values of these solutions were recorded at 488 nm. From the calibration curve constructed, molar absorbance coefficient of adriamycinone was determined as 15551 $L \cdot mol^{-1} \cdot cm^{-1}$ (Figure A.1). To determine total DOX content of the conjugates, approximately, 0.25 mg of sample (mPEG-DOX and mPEG-AT3-DOX) was dissolved in 250 µl of 1N HCl and hydrolyzed at 50 °C for 2 hours. After cooling, 750 µl of DMSO was added and absorbance of the solution was measured at 488 nm. The total DOX amount of the samples (in terms of mmols of DOX conjugation per mmol of COOH group) was determined using the following equations:

$$\%\ DOX\ amount = \frac{C\ (\frac{mmol}{ml}\ of\ DOX\ measured)}{C\ (\frac{mmol}{ml}\ of\ the\ conjugate)} \times 100\%$$

$$C\ \left(\frac{mmol}{ml}\ of\ DOX\ measured\right) = \frac{Absorbance\ measured\ at\ 488\ nm}{15551\ \frac{ml}{mmol\ cm} \times 1\ cm}$$

$$C\ \left(\frac{mmol}{ml}\ of\ the\ conjugate\right) = \frac{Mass\ concentration\ of\ the\ conjugate\ (\frac{mg}{ml})}{MW\ of\ the\ conjugate\ (\frac{mmol}{mg})}$$

All UV-Vis measurements were performed using a Perkin Elmer Lambda-45 model UV-Vis spectrophotometer.

3.3.5. Size Measurement

Size distribution and stability of the conjugates were determined by using dynamic light scattering method. The experiments were carried out on a Malvern ZetaSizer Nano ZS90 model instrument. 1.5 mg/ml of the samples was dissolved in either of the following buffers; 10 mM phosphate buffer with 150 mM NaCl at pH 7.4 or 10 mM acetate buffer with 150 mM NaCl at pH 5.0. The solutions were filtered using a regenerated cellulose filter with 0.2 µm pore size and equilibrated at 25 ^{o}C for at least

10 minutes prior to measurements. For each sample, three measurements were recorded. Diffusion coefficients of the samples were determined using CONTIN method and converted to the hydrodynamic diameters using Stoke-Einstein equation by the software of the instrument. To assess stability of the DOX-conjugated drug delivery systems, two more measurements were taken; one at the end of 24 hours and the other at the end of 24 hours 48 hours upon incubating the samples at 37 °C.

Atomic force microscopy (AFM) images of mPEG-DOX and mPEG-AT3-DOX were obtained using a Digital Instruments- MMSPM Nanoscope lV instrument. Freshly cleaved mica substrate was exposed to UV light further cleaning its surface. The sample (mPEG-DOX or mPEG-AT3-DOX) was dissolved in deionized water at a concentration of ~ 1.5 mg/ml. After filtering (0.2 μm, regenerated cellulose filter) 2 μl of the solution was applied to the plate and diluted at 1:5 ratio by adding 8 μl filtered deionized water on mica plate. In another sample preparation method, 1 μl of filtered mPEG-AT3-DOX at a concentration of 0.15 mg / ml were directly applied onto the cleaned mica plate. The mica plates were dried at room temperature while protected from light, and the images of samples were taken in tapping mode using a silicone tip. 2D and 3D AFM images, particle size distribution and absolute height analysis were obtained using NanoScope Analysis software.

3.3.6. Drug Release

DOX release curves of the DOX-conjugated samples were obtained by using dialysis method (Lee et al., 2003). Approximately, 0.75 mg sample (mPEG-DOX or mPEG-DOX-AT3) was dissolved in 0.5 ml of the appropriate buffer (10 mM phosphate buffer with 150 mM NaCl at pH 7.4 or 10 mM acetate buffer with 150 mM NaCl at pH 5.0 or 50 mM sodium acetate buffer with 150 mM NaCl, 1 mM EDTA, 5 mM L-cysteine at pH 5.0 for cathepsin B containing experiment). To get the enzyme-induced drug release profile of mPEG-AT3-DOX, 5 μl of cathepsin B solution (0.53 mg/ml) was added to the solution. The solutions were transferred to a membrane tubing with a MWCO of 3.5 kDa and the dialysis tubings, then were placed in a 20 ml vial containing 12.5 ml of the appropriate buffer solution. The cap of vial was wrapped using parafilm to prevent evaporation. The vial was placed in an incubator at 37°C and shaked at 150 rpm. 100 μl of mixture was taken from each vial at specific intervals (1,

3, 6, 10, 24, 48, 55 and 72 hrs.) and 100 µl of fresh buffer was replaced to keep the total volume constant. Amount of released DOX from carrier systems (mPEG-DOX and mPEG-AT3-DOX) was determined via fluorescence emission intensity measurements at 590 nm with an excitation wavelength of 480 nm. DOX calibration curves used are given in Figure A.2, Figure A.3 and Figure A.4. % DOX release was calculated using the following equations:

$$DOX\ released\ \% = \frac{C_t\ (mmol\ of\ DOX\ released\ at\ time\ t)}{C_i\ (mmol\ of\ DOX\ in\ the\ \ conjugate\ initially)} \times 100\ \%$$

$$C_i = \frac{1.5\ \frac{mg}{ml}\ conjugate \times 0.5\ ml}{MW\ of\ the\ conjugate\ (\frac{mg}{mmol})} \times \frac{DOX\ conjugation\ \%}{100\ \%}$$

$$C_t = \frac{Fluorescence\ intensity\ at\ 590\ nm}{\varepsilon_{590}\ \left(\frac{ml}{mmol\ cm}\right) \times 1\ cm} \times 12.5\ ml$$

where ε_{590} is the slope of the calibration curve.

All the fluorescence measurements were performed using a VarioSkan Flash Multimode Reader (Thermo Scientific) model microplate reader. Drug release profile of the samples were constructed based on two independent experiments for each sample.

3.3.7. Cytotoxicity Test

Cytotoxicity of the samples was evaluated by MTT method using human lung adenocarcinoma epithelium (A549) and human prostate (PC3) cell lines. MTT assay was applied after ensuring the confluency greater than 80% by area of cancer cells and the desired morphology of PC3 and A549 cell lines given Figure 17 and Figure 18, respectively. Both cell lines were grown in RPMI 1640 medium containing 10% FBS and 50 µg/ml gentamycin.

In a typical MTT assay, 90 µl aliquots of the cells (1 x 10^4 cells/well) were seeded in a 96-well (8 x 12) tissue culture microplate and incubated at 37 °C in 5% CO_2 atmosphere for 24 hrs. After the incubation, 10 µl of sample (DOX-conjugated systems

or free DOX) dissolved in sterile PBS were added to the wells at different concentration. Sterile PBS was used as a control sample. % Viability of DOX-free samples was determined at a single concentration by adding 10 µl of sample with 15000 µg/ml or 7500 µg /ml concentration to the microplates for PC3 and A549 respectively.

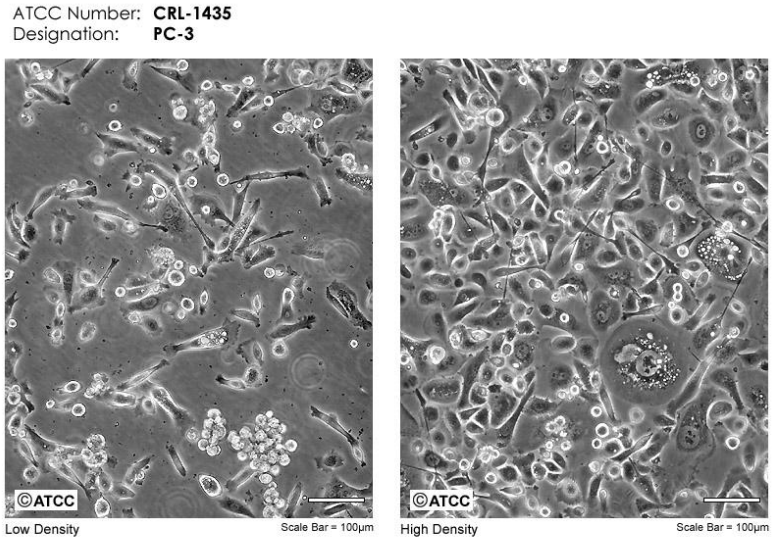

Figure 17. Expected morphology of PC3
(Source: https://www.lgcstandards-atcc.org/~/media/Attachments/2/6/1/7/1753.ashx).

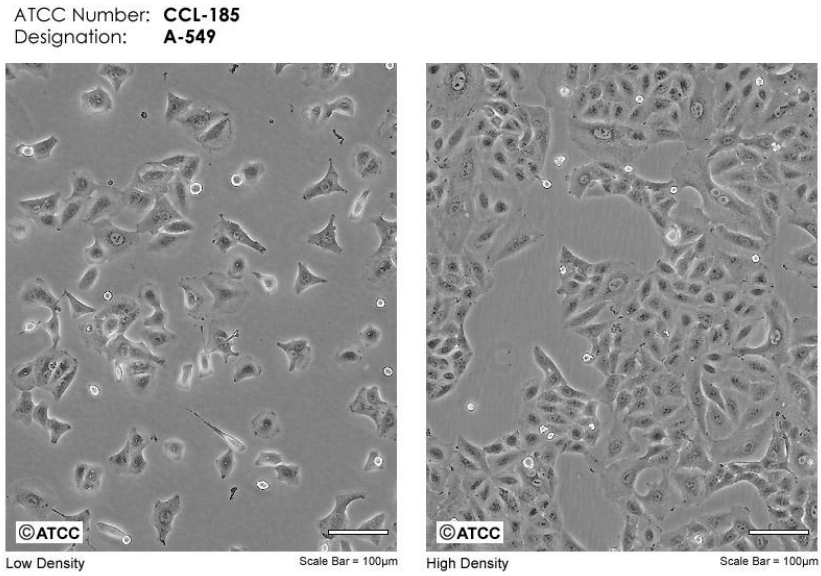

Figure 18. Expected morphology of A549
(Source: https://www.lgcstandards-atcc.org/~/media/Attachments/D/B/B/1/1813.ashx).

Free DOX concentrations were varied between 10-1000 µg/ml for PC3 and 1-1000 µg/ml for A549. mPEG-DOX and mPEG-AT3-DOX were added to the wells at concentrations of 15-7500 µg/ml and 7.5-7500 µg/ml for PC3 and A549, respectively.

Five independent experiments were performed for each concentration. The plates were incubated for further 24 hr and 48 hr at the identical conditions. At the end of 24 hrs or 48 hrs. 10 µl of MTT (5 mg/ml) in sterile PBS was added to each well and then, microplates were incubated for 3 more hr. In the following step, microplates were centrifuged at 1800 rpm for 5 min and supernatants were poured and the microplates were blotted with a napkin. Finally, the empty wells were filled with 100 µl of DMSO and shaken at 150 rpm for 5 min. Absorbance values of each well were measured at 590 nm (reference wavelength; 690 nm) using Thermo Scientific, VarioSkan Flash Multimode Reader.

MTT assay is a colorimetric test for assessing cell metabolic activity of mitochondrial dehydrogenase that is a conversion of tetrazolium salts to the purple tetrazolium formazan crystals (Figure 19). Thus, viable cells show superior absorbance value because of the darker purple color. Calculation of the % viability was given below.

$$viability\ \% = \frac{Absorbance\ of\ the\ sample\ at\ 590\ nm}{Absorbance\ of\ the\ control\ (PBS)\ at\ 590\ nm}\ \text{x}\ 100\%$$

Absolute IC_{50} values of the samples were determined as a concentration that corresponds to 50% of viability by using cubic spline interpolation method provided by Mathematica software. DOX equivalent IC_{50} values of the conjugates were obtained from the equation as;

$$DOX\ equivalent\ IC_{50}\ value = \frac{IC_{50}\ value\ of\ the\ conjugates\ \text{x}\ MW_{DOX}\left(\frac{g}{mol}\right)\text{x}\ \%\ DOX\ amount}{MWconjugate\ \left(\frac{g}{mol}\right)}$$

where the unit of IC_{50} value of the conjugates is $\frac{\mu g\ conjugate}{ml}$.

Finally, statistical analysis of cytotoxicity of DDS was carried out using independent two-sample t-test method on Minitab software. p-values less than 0.05 were considered to be statistically significant difference.

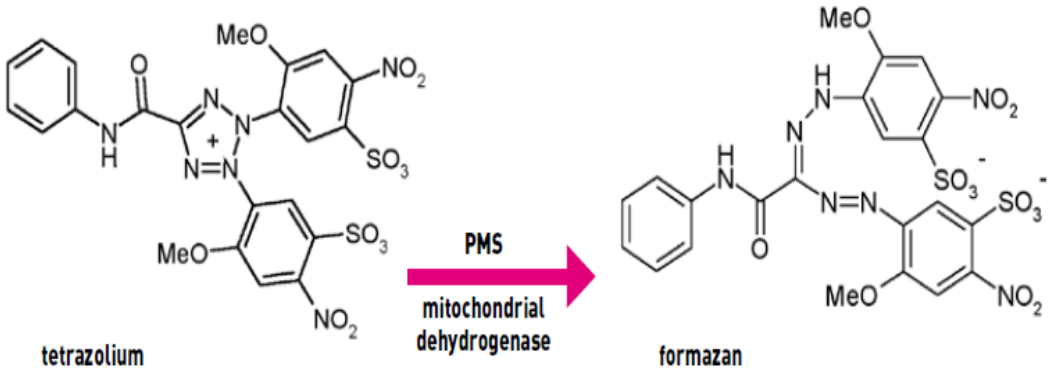

Figure 19. Conversion of tetrazolium salts to formazan

CHAPTER 4

RESULTS AND DISCUSSIONS

4.1. Preparation of mPEG-DOX

In this drug delivery system, DOX was conjugated to the carrier system via a stable amide linkage. mPEG-DOX conjugate, which was synthesized for control system to mPEG-peptide-DOX conjugate was obtained by the coupling reaction shown in Figure 15 between the amine group of DOX with mPEG-propionic acid. mPEG was used to increase the blood circulation time of the carrier system. Characterization of mPEG-DOX system is given in Section 4.3.

4.2. Preparation of mPEG-Peptide based DDS

4.2.1. Peptide (AT3) Synthesis

The *de novo* peptide, AT3, has a sequence of $CG_3H_6R_2ALALG_3E$. In the design of this peptide, cysteine (C) containing thiol functionality (SH) at the N-terminal was used to serve as a PEG attachment site via Michael addition reaction. Six histidines (H) were incorporated to the peptide sequence to impart pH responsiveness property due to its pK_a value around 6.0. RRALAL sequence functions as a substrate for cathepsin B enzyme. Glutamic acid (E) having COO^- functional group is placed at the C-terminus of the peptide to attach DOX. Glycines (G) were placed next to C and E to minimize steric effects during conjugation reactions as G is the smallest amino acid.

To confirm the purity of AT3, MALDI-MS and HPLC were used and the results are shown in Figure 20 and Figure 21 respectively.

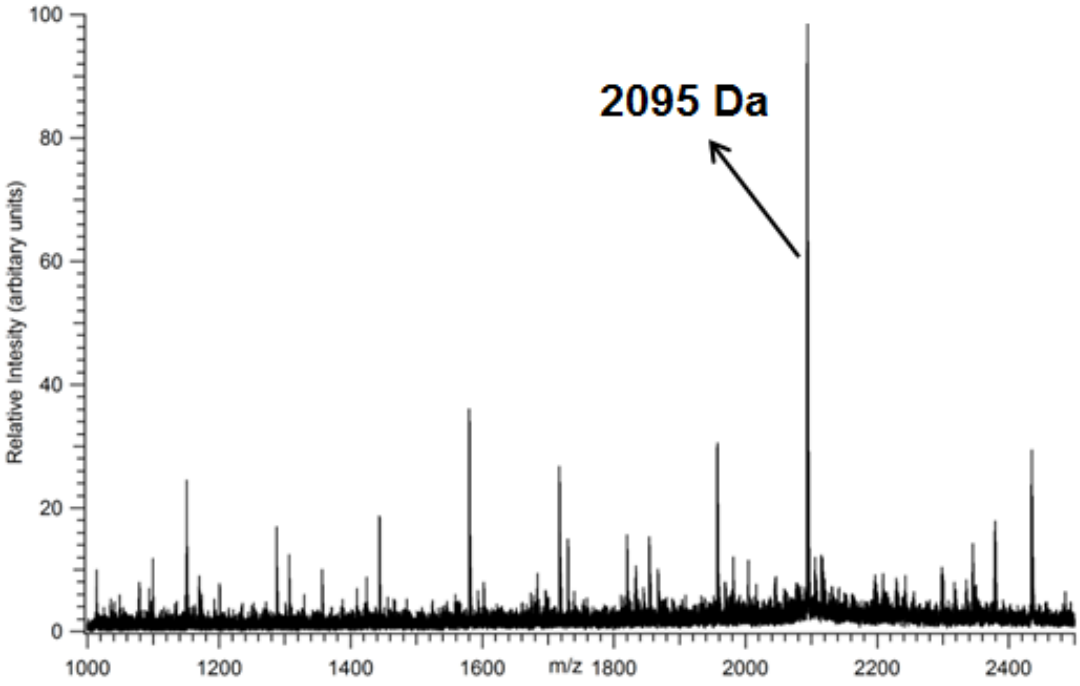

Figure 20. MALDI-TOF MS spectrum of AT3 peptide.

In the mass spectrum, the peak with the highest intensity observed at 2095 Da corresponds to AT3 peptide (theoretical molar mass of the peptide 2096 Da) Additionally, relatively small peaks with lower molecular weight range can be attributed to short peptide fragments resulted from inefficient coupling reactions during synthesis.

A major peak around 14.9 min in HPLC elution curve demonstrates that peptide was obtained at high purity (Figure 21). Thus, both MALDI-MS and HPLC chromatogram clearly indicate that AT3 peptide was synthesized with acceptable purity. For this reason, in the next step AT3 was conjugated to mPEG without any purification step.

4.2.2. PEG-Peptide Conjugation

Purity of the mPEG-AT3 conjugate was assessed by HPLC and MALDI-MS. As indicated in chromatograms given in Figure 21, mPEG-maleimide, peptide and mPEG-AT3 eluted at 38.9, 14.9 and 32.4 min respectively due to difference in their

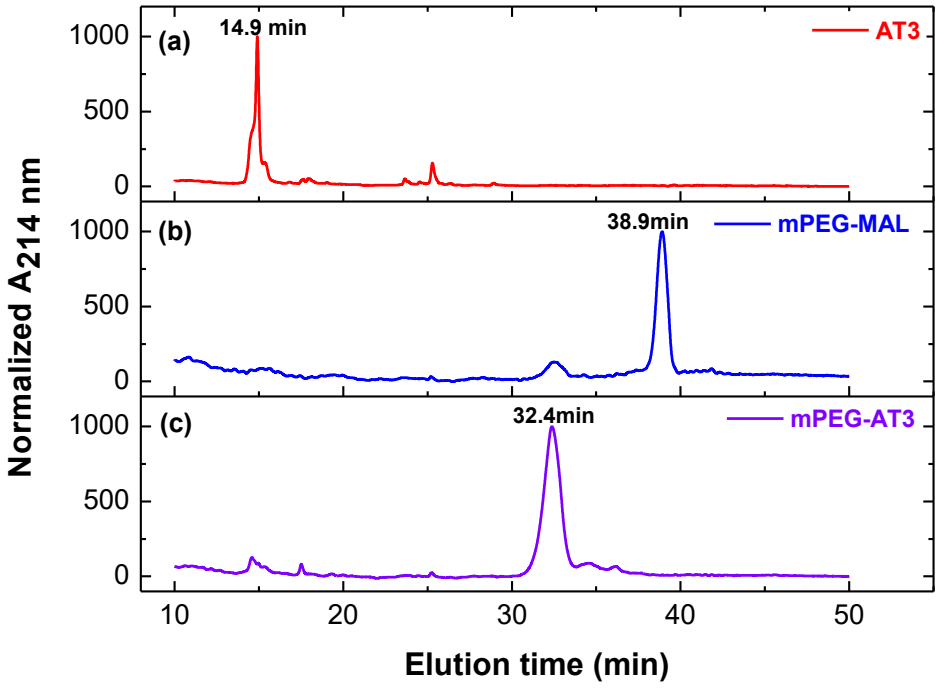

Figure 21. HPLC Curves of (a) AT3, (b) mPEG-MAL and (c) mPEG-AT3.

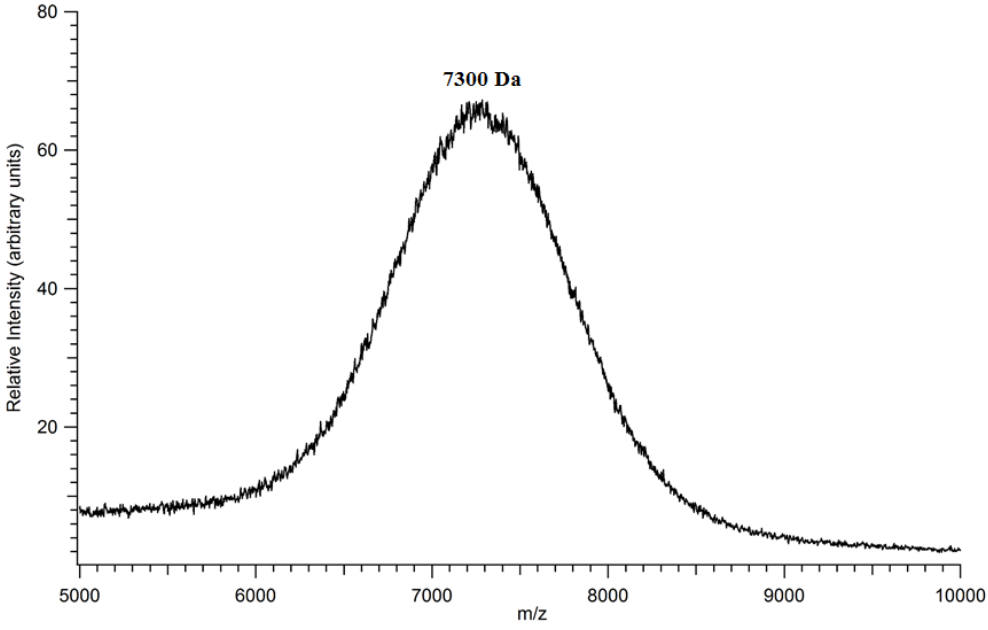

Figure 22. MALDI-TOF Mass Spectrum of mPEG-AT3.

hydrophobicity. No significant fraction that corresponds to the peptide or mPEG-MAL was observed in the chromatogram of mPEG-peptide conjugate, suggesting that the conjugate have high purity. Molar mass of mPEG-peptide conjugate was determined by using MALDI-TOF analysis. As can be seen in the mass spectrum of the conjugate, the peak was observed around 7300 Da (Figure 22) very close to its theoretical value (~ 7100 Da, i.e. $M_{peptide}$=2096 Da and M_{PEG}=5000 Da). There is no significant difference between experimental mass and the theoretical mass. This result shows that, the conjugation reaction was performed successfully.

PEGylation of AT3 was also confirmed by FTIR spectroscopy by comparing the fingerprints of mPEG-MAL, AT3 and the conjugate (Figure 23). It can be clearly seen that, the conjugate has FTIR spectrum that contains bands from parent molecules, mPEG-MAL and AT3. For example, the C-H stretching band of PEG backbone at about 2900 cm^{-1} was also observed in the FTIR spectra of the conjugate. Likewise, amide I and amide II bands of AT3 appeared in 1500 and 1700 cm^{-1} region were also detected in the FTIR pattern of the conjugate. Therefore, these characterization methods indicated that mPEG-peptide conjugate was synthesized and isolated successfully.

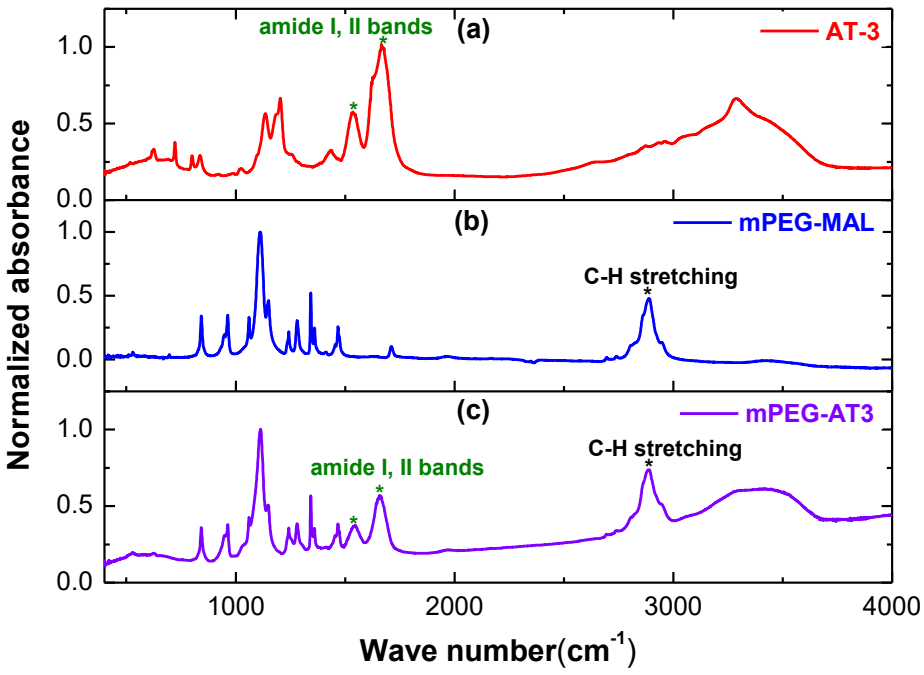

Figure 23. FTIR Spectra of (a) AT3, (b) mPEG-MAL and (c) mPEG-AT3.

4.3. Conjugation of DOX to mPEG-Peptide based DDS

After conjugating DOX molecules to the carrier molecules, amount of DOX incorporated into the carrier systems was determined and results are summarized in Table 2.

Table 2. DOX conjugation yield and percentage of carrier systems.

Sample	Yield %	DOX %*
mPEG-DOX	72 ± 19	109 ± 5
mPEG-AT3-DOX	76 ± 5	187 ± 8

* Moles of DOX / moles of COOH group x 100%

Surprisingly, moles of DOX in the composition of the carrier systems was found to be higher than moles of available carboxylic acid groups suggesting that there might be free DOX in the isolated carrier systems. In order to determine free DOX content of the conjugate with highest apparent DOX content, mPEG-AT3-DOX, was injected to an HPLC column at a concentration of 1.5 mg / ml (total DOX amount = ~ 200 μg / ml, expected free DOX amount = 100 μg / ml). Its elution profile was monitored at 220 nm and 480 nm and compared with that of free DOX. HPLC chromatograms of free DOX and mPEG-AT3-DOX are given in Figure 24 and Figure 25, respectively. Unfortunately, the free DOX could not be detected in the visible region, but a small peak was observed at 12.6 min at 220 nm. In the HPLC curves of mPEG-AT3-DOX given in Figure 27, a large peak at 16.7 min, a small peak at 18.4 min and a broad peak at 24.7 min were observed at both 220 nm and 480 nm. These peaks appeared both at 220 nm and 480 nm indicate that these 3 fractions definitely contain DOX. The absence of any other peak at 220 nm indicates that DOX conjugation to mPEG-AT3 was almost completed and the amount of free DOX is below the detection limit of the device. The peak at 16.7 min represents the mPEG-AT3-DOX fraction. The other two peaks correspond to the different components that can be resulted from side reactions. It was reported that PyBOP can also act as a catalyst in the esterification reactions between the carboxylic acid and alcohol groups (Coste et al.; 1995). Therefore, it is also possible that conjugation of DOX to mPEG-AT3 via ester linkage occurred as a result of the reaction between COOH of mPEG-AT3 conjugate and OH group of DOX.

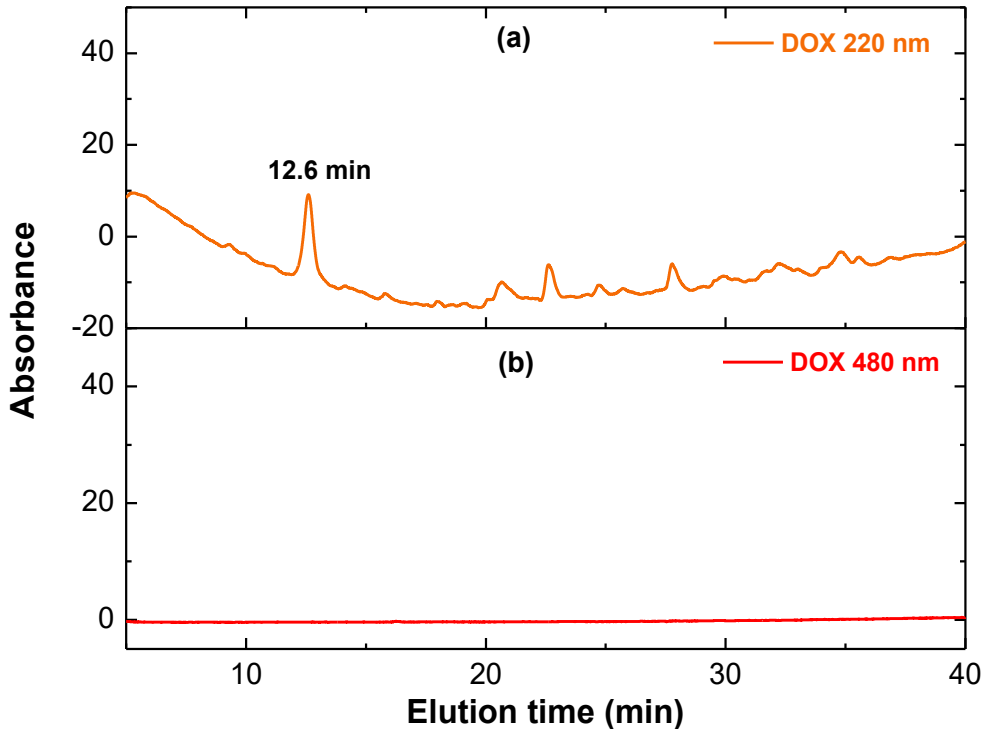

Figure 24 HPLC curves of free DOX at 220 nm and 480 nm.

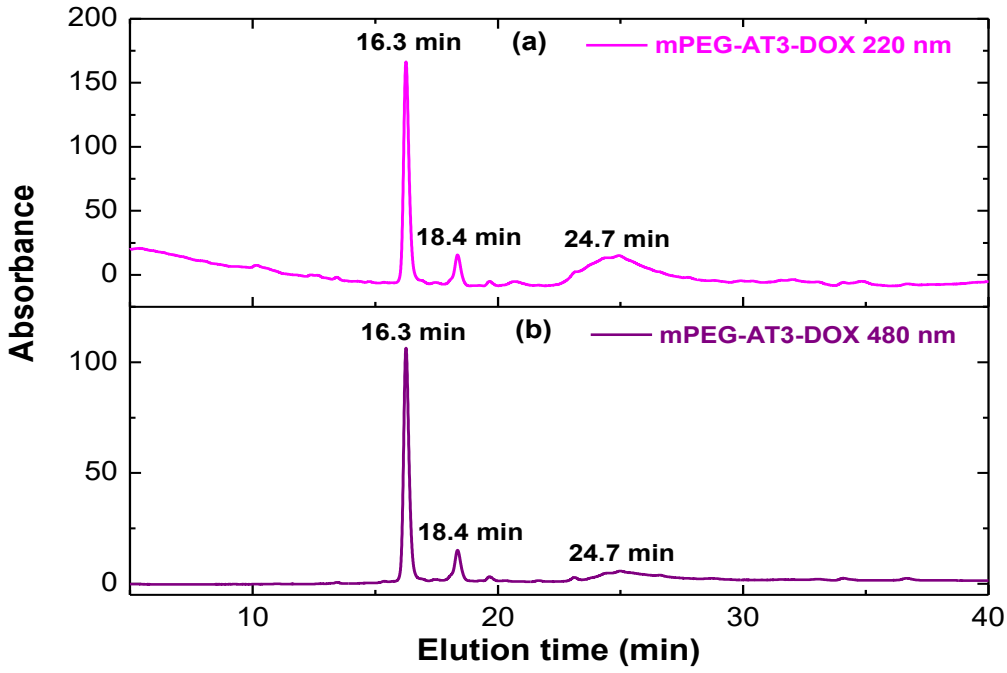

Figure 25 HPLC curves of mPEG-AT3-DOX at 220 nm and 480 nm

4.4. Characterization of DDS

4.4.1. Size Measurement

Size distribution and stability of the drug delivery systems (mPEG-DOX and mPEG-AT3-DOX) at 37 ^{o}C were determined by using dynamic light scattering. Size measurements of the AT3 peptide, mPEG-MAL and mPEG-AT3 conjugate were also performed to clarify the aggregation state of the DOX conjugated carrier systems. As shown in Figure 26, average sizes of AT3, mPEG-MAL and mPEG-AT3 were measured as 1.7 ± 0.4 nm, 2.9 ± 0.2 nm and 5.2 ± 0.4 nm, respectively. The size of mPEG-MAL was about 1 nm less than the theoretical value (4.4 nm) and mPEG-COOH having the same molecular weight (Balcı, 2016). The size of mPEG-AT3 was measured very close to the sum of the mPEG and peptide sizes independent of pH. These results show that mPEG-AT3 has no aggregation tendency and no pH responsive property.

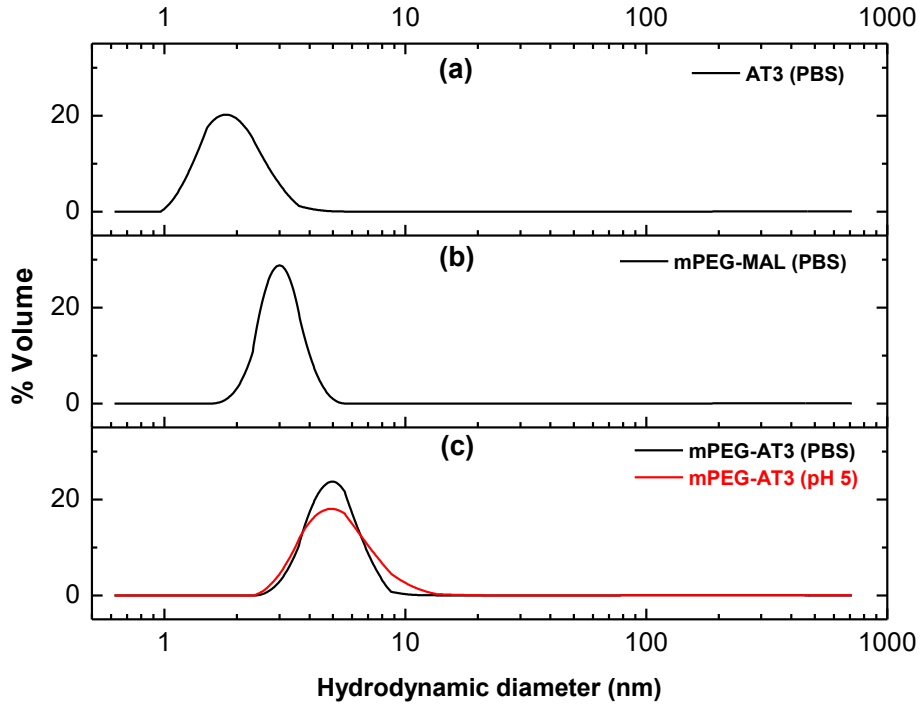

Figure 26. Size distributions of (a) AT3, (b) mPEG-MAL, and (c) mPEG-AT3.

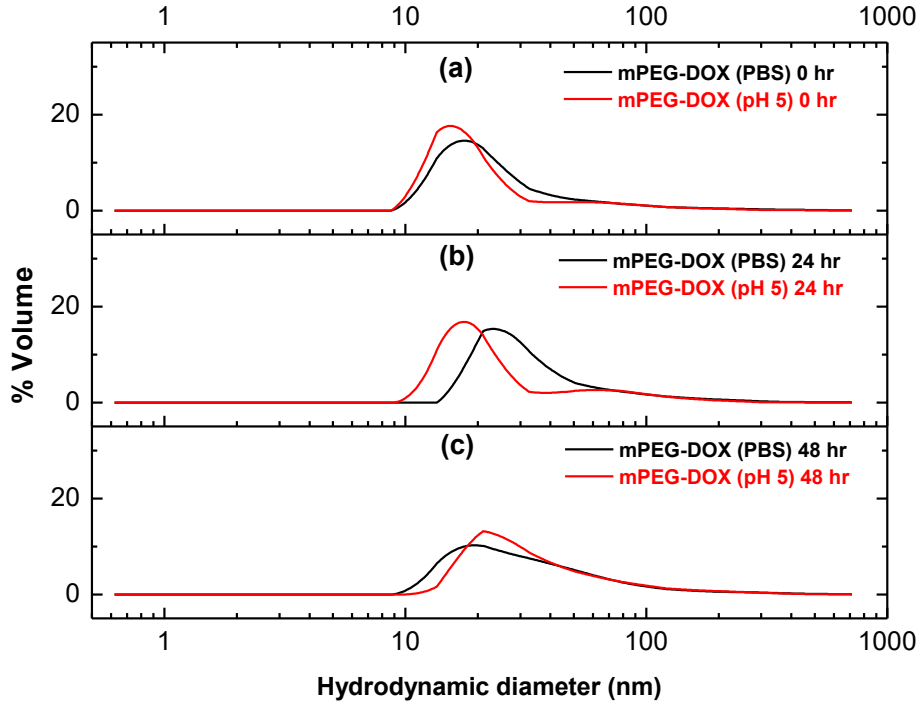

Figure 27. Size distributions of mPEG-DOX measured at (a) 0 hr, (b) 24 hr, and (c) 48 hr.

Average hydrodynamic diameter of mPEG-DOX was determined as 15 ± 3 nm and 19 ± 2 nm at pH 5 and 7.4 (PBS), respectively (Figure 27). This value is more than twice of the size of the mPEG indicating that mPEG-DOX system tends to aggregate. DOX was shown to have hydrophobic character as it could be incorporated into hydrophobic poly(caprolactam) (PCL) block of a PEG-PCL-PEG micellar system (Cuong et al.; 2011). Thus, the carrier system, mPEG-DOX, composed of hydrophobic DOX and hydrophilic mPEG is likely to form aggregate structures with DOX in the core of the DDS and PEG molecules at surface. As the sizes of mPEG-DOX measured initially, after 24 h, and 48 hr at both neutral pH and pH 5 are not different from each other considering standard deviation, the DDS aggregates can be considered to be stable.

Size distributions of mPEG-AT3-DOX measured at different pH values and time intervals are given in Figure 28. Initially, mPEG-AT3-DOX showed bimodal size distributions centered at ~ 15 and ~30 nm, independent of pH. After 48 hours the average size shifted to 30 nm for both pH values. Hence, the number of histidines in the structure seems to be not enough to impart pH responsiveness to the carrier system.

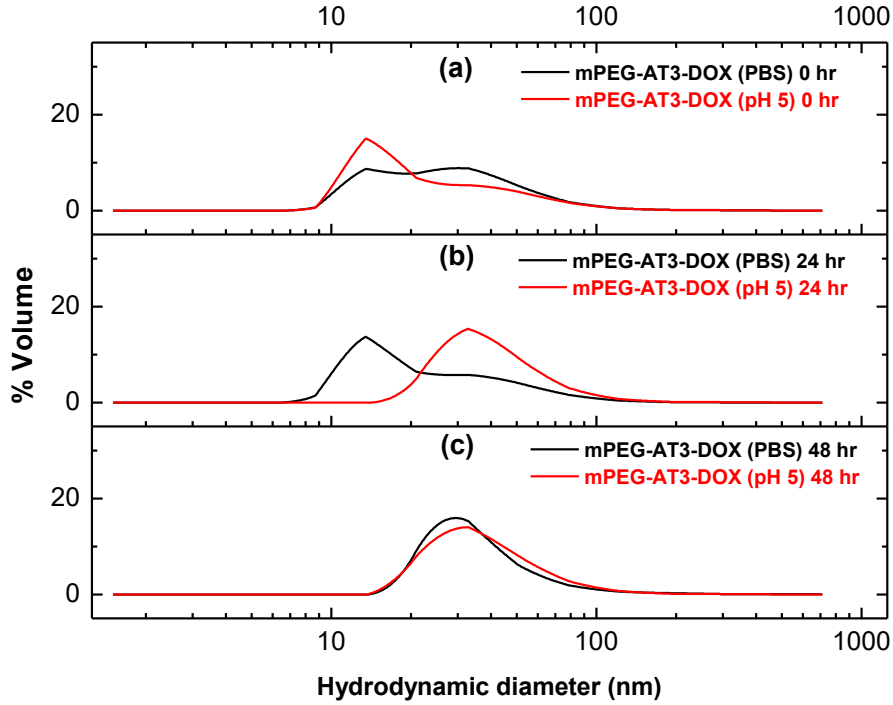

Figure 28. Size distributions of mPEG-AT3-DOX measured at (a) 0 hr, (b) 24 hr, and (c) 48 hr.

Unlike the behavior of mPEG-DOX, which forms stable aggregates at pH 7.4 at about 19 ± 2 nm, increase in the aggregation tendency of mPEG-AT3-DOX as time proceeds can be attributed to its higher unbound DOX content compared to mPEG-DOX system. The components that constitute the micelle systems are constantly exchanging between different micelles with mechanisms such as single chain attachment or fusion / fission. This change of the reaction kinetic is so fast that it can only be detected by changing temperature or pressure (Lund et al.; 2013). Therefore, the increase in size of the mPEG-AT3-DOX system over time can be explained by the increase in the mobility of the molecules and the speed of fusion of the micelles, by increasing the temperature to 37 °C. DOX molecules that are not conjugated to the mPEG-AT3 system in the mPEG-AT3-DOX aggregates are much smaller than polymer chains so increasing the temperature from room temperature to 37 °C increases mobility of unbound DOX molecules to a higher extent compared to polymer chains. For this reason, mPEG-DOX, which includes less free DOX than mPEG-AT3-DOX, exhibited much more stable behavior.

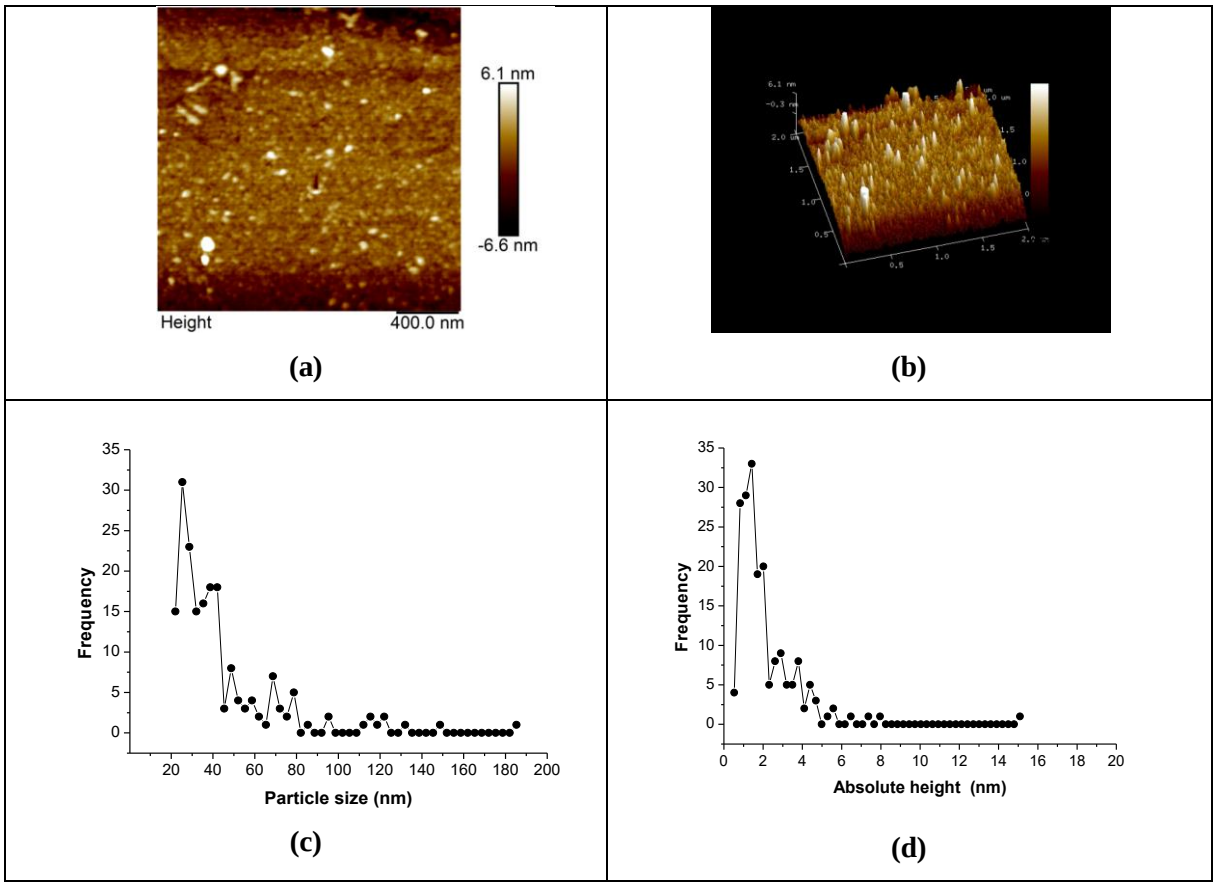

Figure 29. AFM images of mPEG-DOX (a) 2-D image, (b) 3-D image, (c) particle size distribution, (d) absolute height distribution.

AFM images of mPEG-DOX and mPEG-AT3-DOX are given in Figures 29 (a-b) and 30 (a-b), respectively. Additionally, particle size and absolute height distribution obtained from the AFM images of mPEG-DOX are shown in Figure 29 (c-d). The 2D AFM image of mPEG-DOX showed that the aggregates have circular or elliptical cross section. In its particle size distribution, it was observed that most of the aggregate population ranged between 25 and 40 nm. Slightly larger size values obtained from AFM image compared to those of dynamic light scattering can be explained by the fusion of the aggregates as a result of increasing concentration during sample preparation and/or interaction of PEG chains with mica substrate thereby spreading on the surface. Height of the aggregates was obtained to be quite low around 1.4-5.5 nm. Similar behavior was also observed for mPEG-PBLA-pyrene system with an average size of 48 nm obtained from DLS. In its AFM image the structures with a circular cross section having slightly higher average size ~ 56 nm were observed. Average height of

these aggregates was determined as ~ 6 nm. Low height of the aggregates was attributed to the spread of the

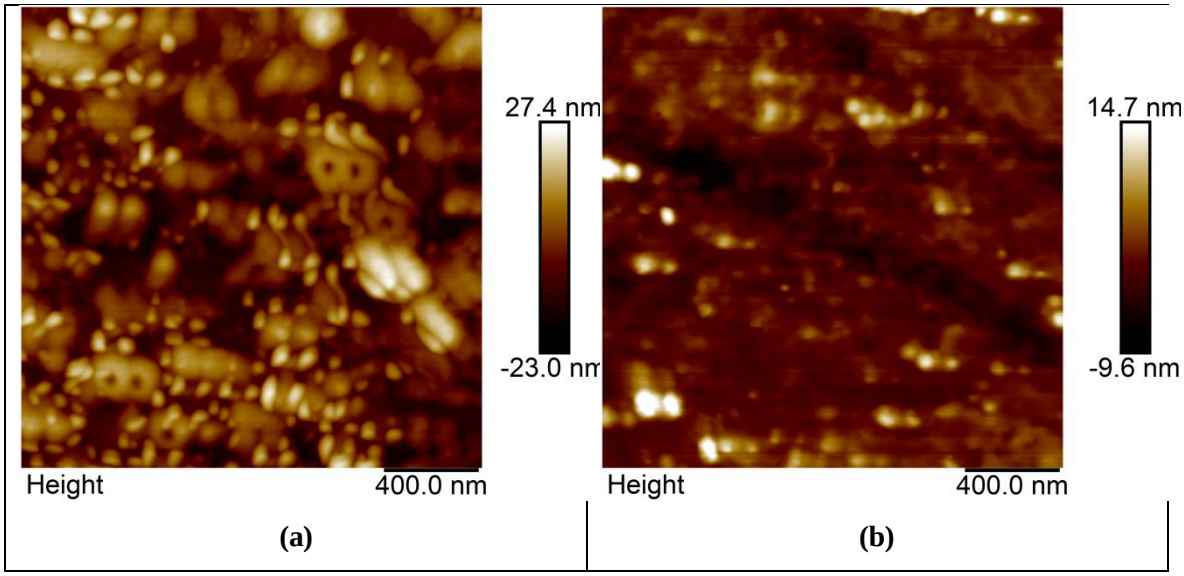

Figure 30. Two-dimensional AFM images of the PEG-AT3-DOX sample (a) diluted 5-times on the plate and (b) diluted 10-times and then added to the plate.

aggregates over mica surface as a result of compression of the structures by cantilever during measurement (Liaw et al.; 1998). mPEG-AT3-DOX aggregates exhibiting an unstable tendency according to DLS results demonstrated strong aggregation tendency likely to be evolved during sample preparation as given in AFM images. To obtain AFM images of mPEG-AT3-DOX, the same method used in mPEG-DOX sample preparation was applied first. In this method, the sample at a concentration 1.5 mg / ml was diluted 5 times on mica plate. As shown in Figure 32 (a), sample size was obtained to be quite large around 100-400 nm. As a second sample preparation method, 10 times diluted sample (C = 0.15 mg/ml) was added to the mica surface. In this method, aggregation tendency is much less than that observed for the first method revealed by ~ 100 nm sized structures but this value is still higher than the size measured by DLS. Thus, it seems that current AFM sample preparation procedures are not suitable for getting decent AFM images of mPEG-AT3-DOX conjugates. Substrates having surface properties different from mica could be used or the image can be acquired in liquid phase to avoid increase in the concentration of the samples upon evaporation during sample preparation over a substrate.

4.4.2. Drug Release Results

DOX release curves of the carrier systems at different conditions are given in Figure 31. Maximum % drug release value of the conjugates was obtained as 8.5 ± 3% without significant differences when the enzyme was not used. mPEG-AT3-DOX, having enzymatic degradation units, showed nearly 17% ± 2 DOX release with in the presence of the cathepsin B.

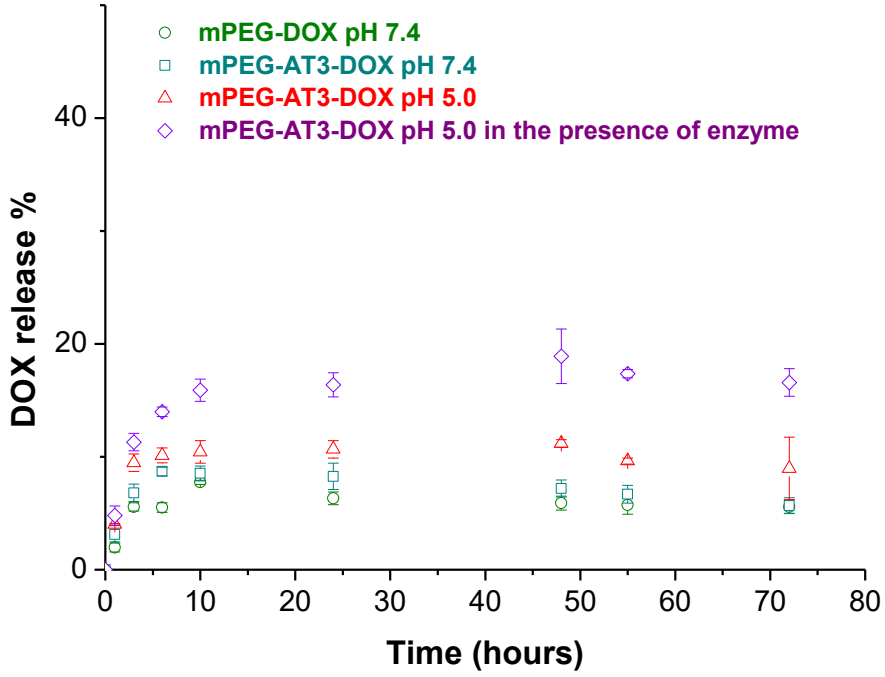

Figure 31. DOX release profile of mPEG-DOX and mPEG-AT3-DOX samples.

Improvement of drug release by the incorporation of enzyme cleavable domains into the structure of the DDS is quite clear but it is, somehow, less than expected. In the system where doxorubicin attached to an albumin-peptide conjugate system containing RRALAL sequence, nearly all of the DOX was released after 24 hours in the presence of cathepsin B (Schmid et al., 2007). Similarly, DOX release from HPMA copolymers-DOX conjugates containing another enzymatic degradation units GFLG group, was increased by 15-30% in the presence of cathepsin B (Etrych et al., 2001). Although no results were reported for aggregation behavior of albumin-peptide-DOX and HPMA-DOX conjugates, aggregation tendency of mPEG-AT3-DOX was accounted for its lower DOX release property. For mPEG-AT3-DOX, it is likely that mPEG molecules

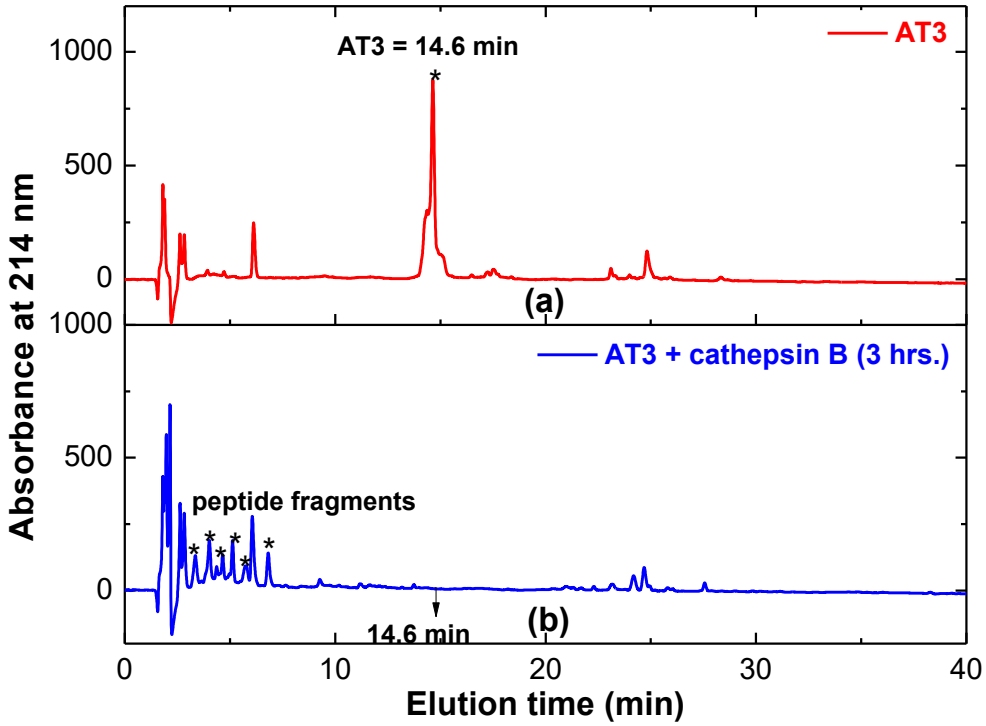

Figure 32. HPLC curves of AT3 peptide (a) before being treated with cathepsin B, (b) after being treated with cathepsin B for 3 hours.

at the surface reduced the interaction of the cathepsin B enzyme with the enzymatic degradation sequences located inner parts of the structure.To confirm this hypothesis, cleavage profile of AT3 peptide with cathepsin B enzyme was monitored by HPLC analysis. As shown in Figure 32, the peak observed at 14.6 min that corresponds to AT3 peptide disappeared completely and new peaks appeared between 3rd and 7th minutes upon incubation of the peptide and cathepsin B. This result confirms that the enzyme shows its activity effectively within 3 hours even though peptide substrate to enzyme ratio in HPLC experiments is 3.75 times higher than that is used in drug release experiments. Thus, according to these results, it seems that the aggregation tendency of mPEG-AT3-DOX is responsible for its lower than expected enzyme-induced DOX release properties.

4.4.3. Cytotoxicity Results

Prior to MTT test, number of cells applied to the wells was optimized to get absorbance values 0.75 and 1.75 at 590 nm. As shown in Figure 33 and 34, 10000 cells/well was determined to be appropriate for both PC3 and A549 cell lines.

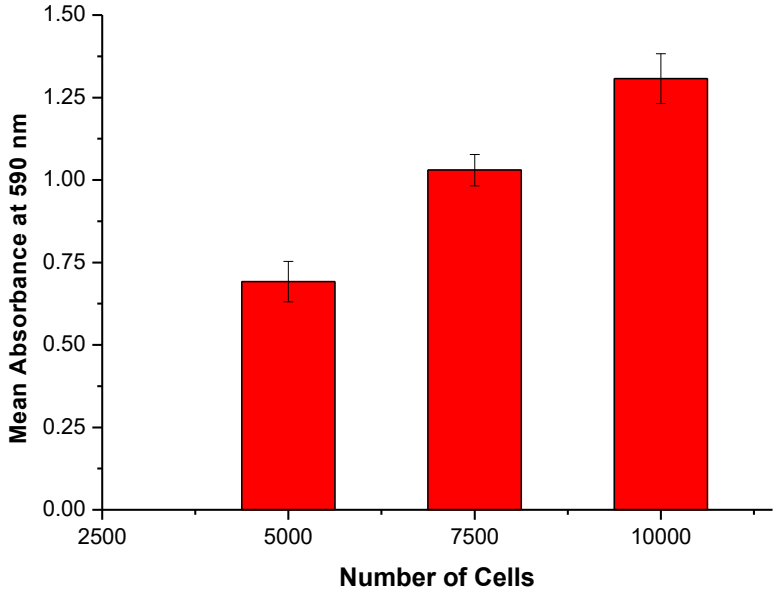

Figure 33. Absorbance values of PC3 cell lines as a function of cells number used in MTT assay.

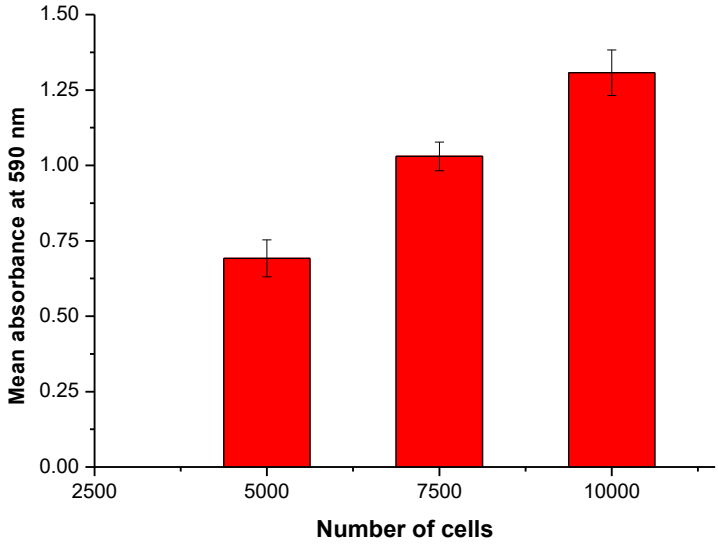

Figure 34. Absorbance values of A549 cell lines as a function of cells number used in MTT assay.

In vitro cytotoxicity of the AT3 peptide, mPEG-MAL and mPEG-AT3 conjugate was tested in the A549 and PC3 cell lines at single concentration. Viability curves obtained at the end of 24 hours and 48 hours are given in Figure 35, 36, 37 and 38. mPEG-MAL did not show a cytotoxic effect similar to mPEG-COOH (Balcı 2016). However, the AT3 peptide and mPEG-AT3 used at a concentration of 1.5 mg/ml showed significant cytotoxicity against PC3 cell line. AT3 and mPEG-AT3 were used at a lower concentration (0.75 mg/ml) in the A549 cell. For this reason, their cytotoxic effects could only be seen at the end of 48 hours. It was reported that many cytotoxic peptides contain positively charged lysine and arginine (Kourie et al., 2000). A previously designed peptide AT1 with a sequence of CGGGHHHHHHGGGE did not show any cytotoxicity against A549 cell line (Balcı 2016). Thus, cytotoxic effect of AT3 is likely due to the arginines in enzymatic degradation unit (RRALAL).

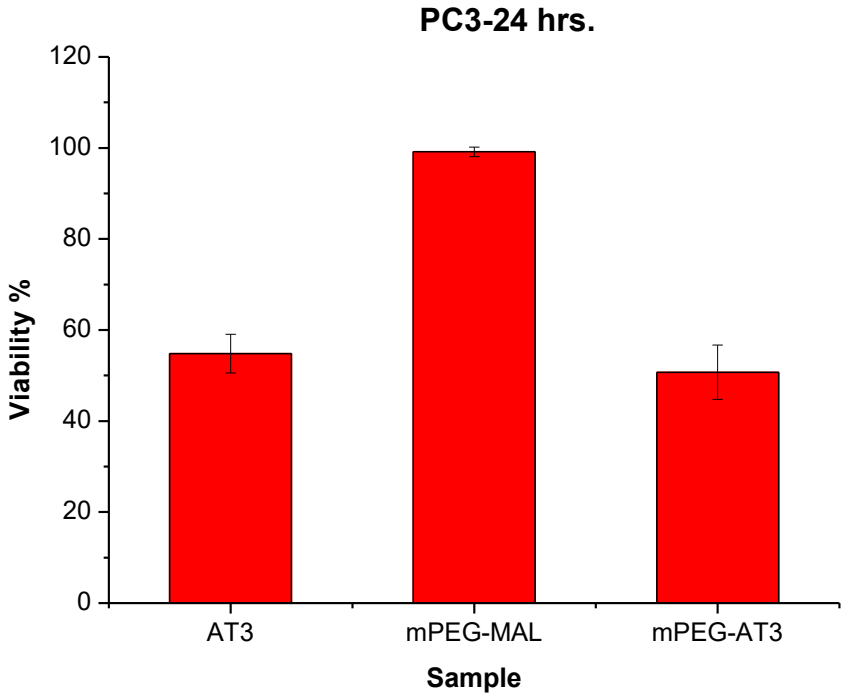

Figure 35. AT3 peptide, mPEG-maleimide, and mPEG-AT3 samples obtained after 24 hours using the PC3 cell line (C = 1.5 mg / ml).

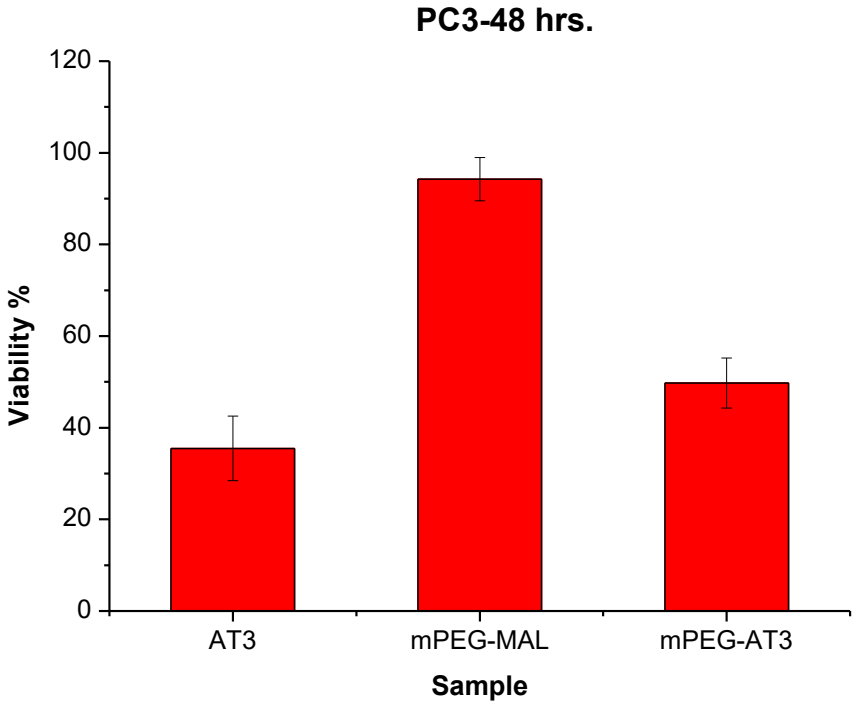

Figure 36. AT3 peptide, mPEG-maleimide, and mPEG-AT3 samples obtained after 48 hours using the PC3 cell line (C = 1.5 mg / ml).

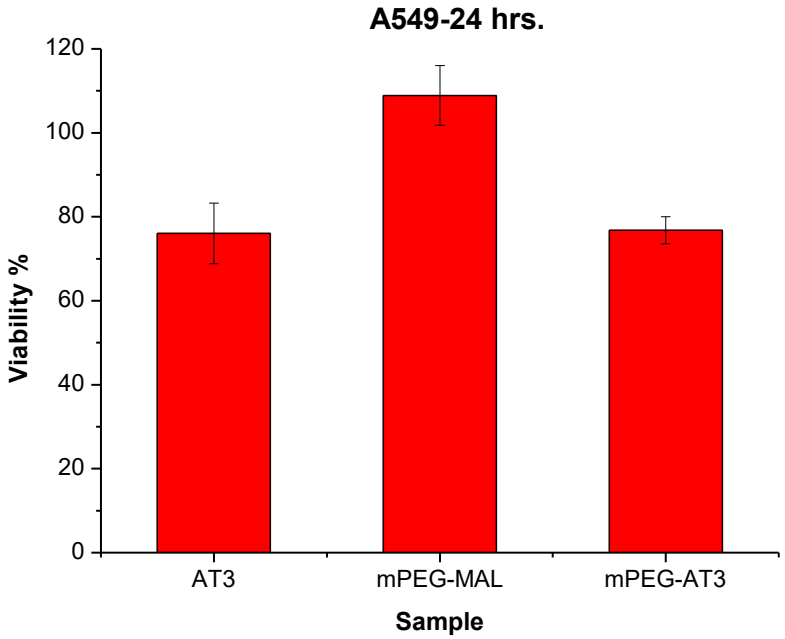

Figure 37. AT3 peptide, mPEG-maleimide, and mPEG-AT3 samples obtained after 24 hours using the A549 cell line (C = 0.75 mg / ml).

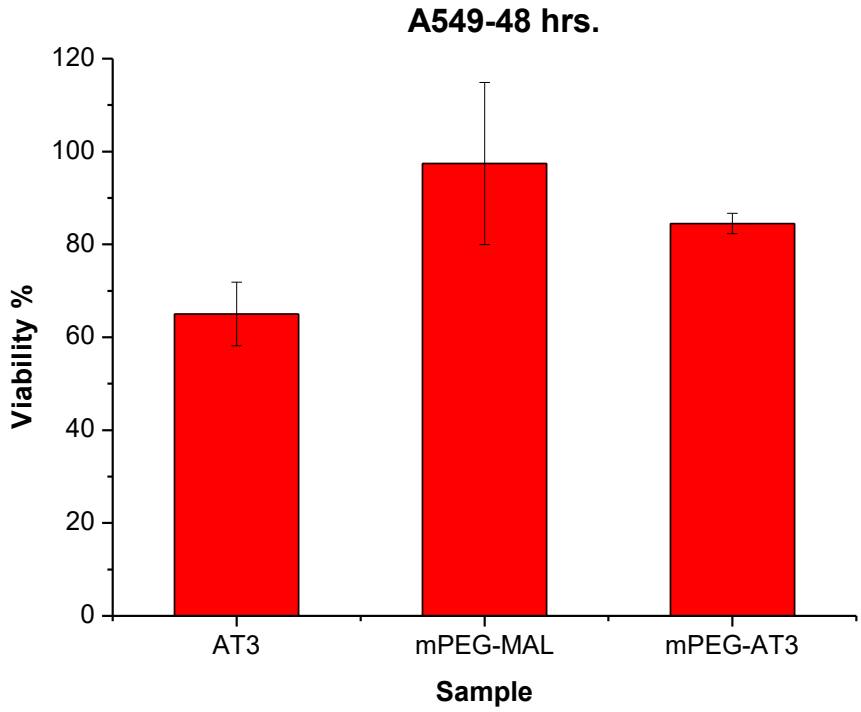

Figure 38. AT3 peptide, mPEG-maleimide, and mPEG-AT3 samples obtained after 48 hours using the A549 cell line (C = 0.75 mg / ml).

Growth inhibition curves obtained at the end of 24 hours and 48 hours of the free DOX, mPEG-DOX and mPEG-AT3-DOX samples are given in Figure 39 and 40 for PC3 and Figures 41 and 42 for A549 cell line. Absolute IC_{50} values of free DOX and carrier systems are summarized in Table 3. Statistical comparison of free DOX and the DDS evaluated based on p-values of independent two-sample t-test is given in Table 4. p-values show that for DOX and mPEG-AT3-DOX pair no statistically significant differences exist in their absolute IC_{50} values obtained at the end of 24 h against both PC3 and A549 cell line. Additionally, IC_{50} values of mPEG-DOX and mPEG-AT3-DOX obtained at the end of 48 h for PC3 cells were also determined to be statistically not different from each other. According to the general trend of IC_{50} values, the cytotoxicity of the samples can be ordered as free DOX ≥ mPEG-DOX-AT3 ≥ mPEG-DOX. No correlation was found between the in vitro cytotoxic effect of DOX release and mPEG-DOX conjugates containing different peptide sequences, and it was reported that free DOX might have an effect on cytotoxicity even though it is present in low amounts (Veronese et al., 2005). Thus, slightly higher cytotoxicity of mPEG-AT3-DOX compared to mPEG-DOX can be attributed to higher content of free DOX in mPEG-AT3-DOX. Additionally, cytotoxicity of AT3 peptide might also contribute to the total cytotoxicity of mPEG-AT3-DOX system.

Table 3. Absolute IC_{50} values of free DOX and the DOX-conjugated DDS.

Sample	**DOX equivalent IC_{50} value (μg/ml)**			
	A549		**PC3**	
	24 hrs.	**48 hrs.**	**24 hrs.**	**48 hrs.**
Free DOX	1.37 ± 0.05	0.60 ± 0.06	1.51 ± 0.07	<1
mPEG-DOX	1.87 ± 0.27	0.80 ± 0.13	3.81 ± 0.72	0.54 ± 0.04
mPEG-AT3-DOX	1.33 ± 0.11	0.72 ± 0.07	1.63 ± 0.80	0.39 ± 0.03

Table 4. Statistical comparison of absolute IC_{50} values of free DOX and the DDS.

Sample pair	**p-value**			
	A549		**PC3**	
	24 hr	**48 hr**	**24 hr**	**48 hr**
DOX and mPEG-DOX	0.023	0.025	0.002	NA*
DOX and mPEG-AT3-DOX	**0.453**	0.023	**0.747**	NA*
mPEG-DOX and mPEG-AT3-DOX	0.014	**0.242**	0.003	0

NA* could not be determined

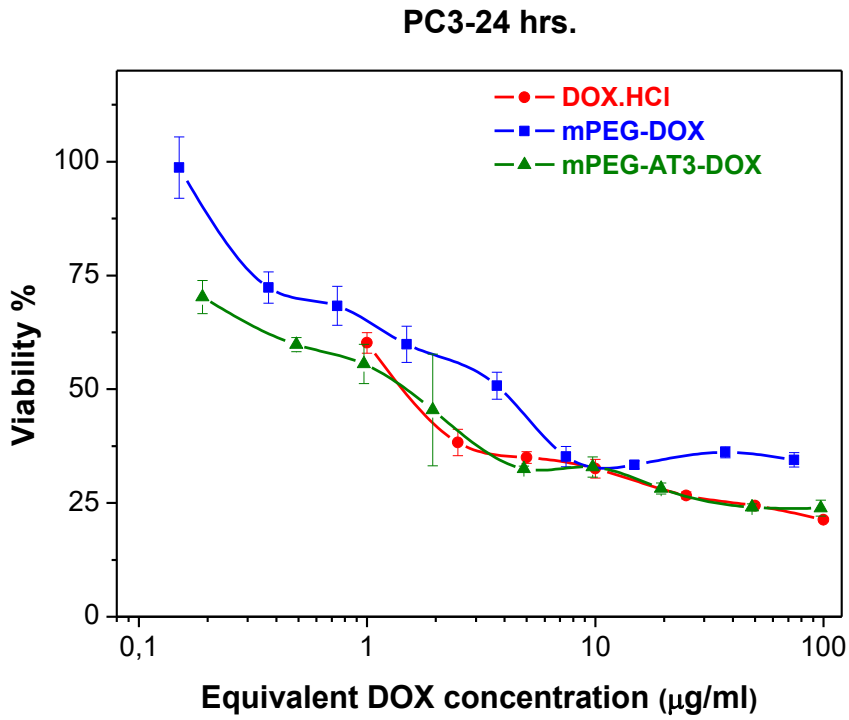

Figure 39. Growth inhibition curves of free DOX and the DOX-conjugated DDS obtained at the end of 24 hours using PC3 cell line.

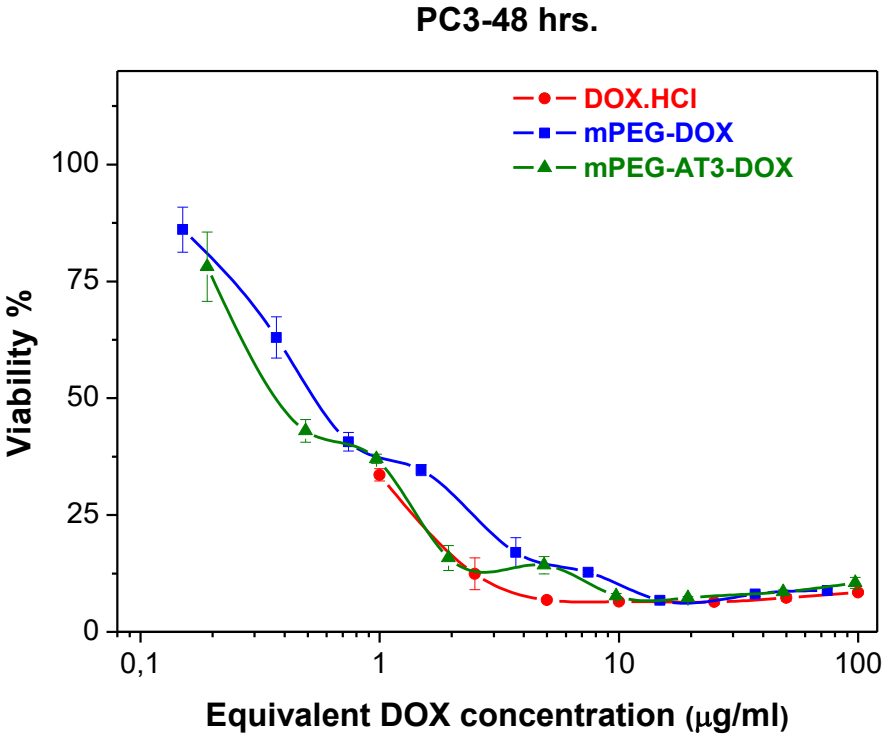

Figure 40. Growth inhibition curves of free DOX and the DOX-conjugated DDS obtained at the end of 48 hours using PC3 cell line.

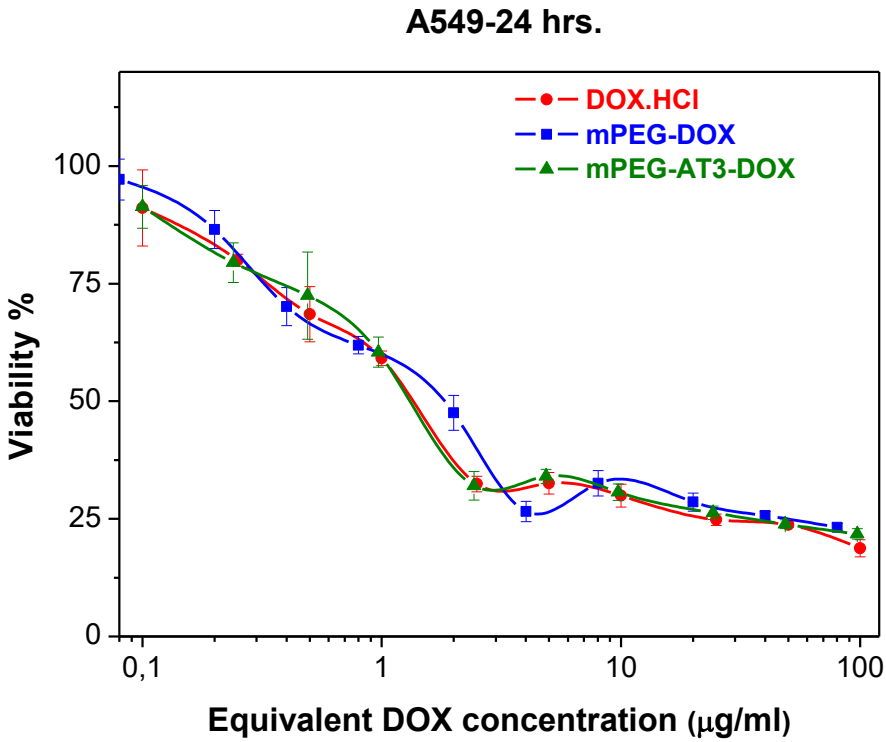

Figure 41. Growth inhibition curves of free DOX and the DOX-conjugated DDS obtained at the end of 24 hours using A549 cell line.

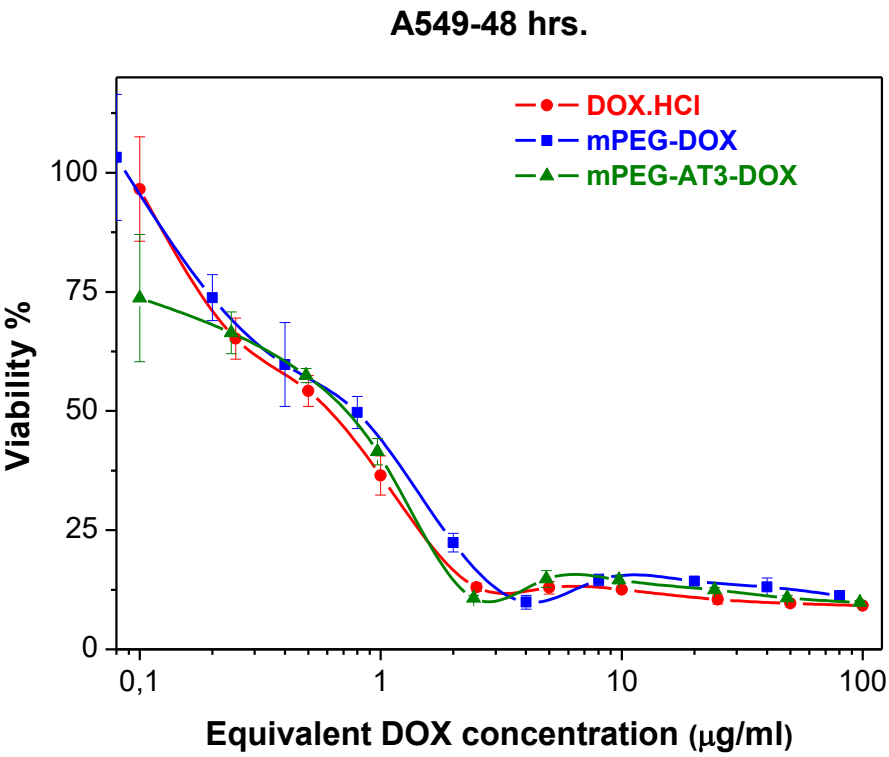

Figure 42. Growth inhibition curves of free DOX and the DOX-conjugated DDS obtained at the end of 48 hours using PC3 cell line.

CHAPTER 5

CONCLUSIONS

In this study, drug delivery systems containing stable amide bond was synthesized. mPEG-AT3-DOX system contains a *de novo* peptide (AT3), which includes enzymatic degradation unit and pH sensitive histidine group. mPEG-DOX conjugate was synthesized as a control carrier system to determine effect of the peptide. Due to the inability to completely remove unbound DOX from the synthesized conjugates, the percent of DOX relative to COOH groups was obtained as ~ 110% and ~ 190% for mPEG-DOX and mPEG-AT3-DOX respectively. Both mPEG-DOX and mPEG-AT3-DOX conjugates showed aggregation tendency. The hydrodynamic diameter of mPEG-DOX was measured as ~ 15-20 nm, while mPEG-AT3-DOX showed two different size distributions at ~ 15 and 30 nm. At the end of 48 hours, there was no change in the size distribution of mPEG-DOX whereas average size of mPEG-AT3-DOX increased to ~ 30 nm. From the DOX release curve, % DOX release amount was obtained below ~ 10% for mPEG-DOX at pH 7.4, mPEG-AT3-DOX at pH 7.4 and pH 5.0 in the absence of enzyme at the end of 72 hours. % DOX release increased to 17 ± 2% for mPEG-AT3-DOX at pH 5.0 in the presence of cathepsin B. This increase is lower than expected when compared to the performance of the other carrier systems containing enzymatic degradation units. HPLC analysis showed that the AT3 peptide treated with cathepsin B was completely cleaved. Thus, modest DOX release profile of mPEG-AT3-DOX can be explained by the lowered interactions of the cathepsin B-RRALAL sequence due to the aggregation tendency of mPEG-AT3-DOX. Thus, it is likely that DOX release rate of mPEG-AT3-DOX can be improved significantly, if pH responsiveness of mPEG-AT3-DOX becomes more pronounced. The cytotoxicity tests showed that mPEG-AT3-DOX conjugate was as toxic as almost free DOX. This observation indicates that AT3 peptide having inherent cytotoxic properties and the unconjugated DOX molecules in the composition of mPEG-AT3-DOX may also contribute to the cytotoxic activity of the mPEG-AT3-DOX conjugate.

Future studies will focus on the improvement of pH sensitivity of the carrier systems and increasing size of the DDS to exploit the EPR effect more efficiently. Increasing number of histidines in the sequence can reduce the aggregation tendency of

the carrier systems at pH 5 by improving the interactions of the enzyme and enzymatically degradable domain of the DDS and hence increasing the rate of DOX release. For current carrier systems, it may be possible to increase the size of the aggregates by reducing the size of the mPEG block. It can also be suggested to use a longer polypeptide block with multiple drug attachment sites instead of a peptide to reach the appropriate size of the carrier system.

REFERENCES

Abou-Jawde R.; Choueiri T.; Alemany C.; Mekhail T. An Overview of Targeted Treatments in Cancer. *Clinical Therapeutics*. **2003**, 25, 2121-2137.

Bae, Y.H.; Park, K. Targeted Drug Delivery to Tumors: Myths, Reality and Possibility. *Journal of Controlled Release*. **2011**, 153(3), 198-205.

Balcı B.; Development of PEG and PEG-peptide Based Drug Delivery Systems. *M.Sc. Thesis, Izmir Institute of Technology*. **2016**.

Brannon-Peppas L.; Blanchette J. O. Nanoparticle and Targeted Systems for Cancer Therapy. *Advanced Drug Delivery Review*. **2004**, 56, 1649-1659.

Chari R.V.J. Targeted Delivery of Chemotherapeutics: Tumor-Activated Prodrug Therapy. *Advanced Drug Delivery Reviews*. **1998**, 31, 89-104.

Chen, W.; Meng, F.; Cheng, R.; Zhong, Z. pH-Sensitive Degradable Polymersomes for Triggered Release of Anticancer Drugs: A Comparative Study with Micelles. *Journal of Controlled Release*. **2010**, 142, 40-46.

Coste, J.; Campagne, J.M. A propos de l'estérification des acides carboxyliques par le BOP ou le PyBOP. *Tetrahedron letters*. **1995**, 36, 4253-4256.

Cuong, N.V.; Jiang, J.L.; Li, Y.L.; Chen, J.R.; Jwo, S.C.; Hsieh, M.F. Doxorubicin-Loaded PEG-PCL-PEG Micelle Using Xenograft Model of Nude Mice: Effect of Multiple Administration of Micelle on the Suppression of Human Breast Cancer. *Cancers*. **2011**, 3, 61.

Devalapally H.; Shenoy D.; Little S.; Langer R.; and Amiji M. Poly(ethylene oxide)-Modified Poly(beta-amino ester) Nanoparticles as a pH-Sensitive System for Tumor-Targeted Delivery of Hydrophobic Drugs: Part 3. Therapeutic Efficacy and Safety Studies in Ovarian Cancer Xenograft Model. *Cancer Chemotherapy and Pharmacology*. **2007**, 59, 477-484.

Doxakis, A.; Maria, A.; Savvas, P.; Zafiroula, I.K. Assessment of the Roles of Cathepsins B, H and L in the Progression of Colorectal Cancer. *Journal of Cancer Therapy*. **2013**, 4, 1-7.

Etrych, T.; Jelinkova, M.; Rihova, B.; Ulbrich, K. New HPMA Copolymers Containing Doxorubicin Bound via pH- Sensitive Linkage: Synthesis and Preliminary in Vitro and in Vivo Biological Properties. *Journal of Controlled Release*. **2001**, 73, 89-102.

Fee, C.J.; Alstine, J.M.V. PEG-Proteins: Reaction Engineering and Separation Issues. *Chemical Engineering Science*. **2006**, 61(3), 924-939.

Feng, S.S.; Chien, S. Chemotherapeutic engineering: application and further development of chemical engineering principles for chemotherapy of cancer and other diseases. *Chemical Engineering Science.* **2003**, 58, 4087-4114.

Gabizon, A.; Shmeeda, H.; Horowitz, A.T.; Zalipsky, S. Tumor Cell Targeting of Liposome-Entrapped Drugs with Phospholipid-Anchored Folic Acid-PEG Conjugates. *Advanced Drug Delivery Reviews*. **2004**, 56, 1177-1192.

Gillies, E.R.; Frechet, J.M.J. Development of Acid-Sensitive Copolymer Micelles for Drug Delivery. *Pure and Applied Chemistry*. **2004**, 76, 1295-1307.

Hu, Q.; Sun, W.; Wang, C.; Gu, Z. Recent Advances of Cocktail Chemotherapy by Combination Drug Delivery Systems. *Advanced Drug Delivery Reviews*. **2016**, 98, 19-34.

Kooijmans, S.A.A.; Fliervoet, L.A.L.; Van der Meel, R.; Fens, M.H.A.M.; Heijnen, H.F.G.; Van Bergen en Henegouwen, P.M.P.; Vader, P.; Schiffelers, R.M. PEGylated and Targeted Extracellular Vesicles Display Enhanced Cell Specificity and Circulation Time. *Journal of Controlled Release*. **2016**, 224,77-85.

Kourie, J.; Shorthouse. A. Properties of cytotoxic peptide-formed ion channels. *American Journal of Physiology-Cell Physiology*. **2000**, 278, C1063-C1087.

Lee, E.S.; Na, K.; Bae, Y.H. Polymeric Micelle for Tumor pH and Folate-Mediated Targeting. *Journal of Controlled Release*. **2003**, 91, 103-113.

Lee E. S.; Na K.; Bae Y. H. Doxorubicin Loaded pH-Sensitive Polymeric Micelles for Reversal of Resistant MCF-7 Tumor. *Journal of Controlled Release*. **2005**, 103, 405-418.

Lee, E.S.; Oh, K.T.; Kim, D.; Youn, Y.S.; Bae, Y.H. Tumor pH-Responsive Flower-Like Micelles of Poly(L-lactic acid)-b-Poly(ethylene glycol)-b-Poly(L-histidine). *Journal of Controlled Release*. **2007**, 123, 19-26.

Liang, X.J.; Chen, C.; Zhao, Y.; Wang P.C. Circumventing Tumor Resistance to Chemotherapy by Nanotechnology. *Methods in Molecular Biology*. **2010**, 596, 467-488.

Liaw, J.; Aoyagi, T.; Kataoka, K.; Sakurai, Y.;Okano, T. Visualization of PEO-PBLA-pyrene Polymeric Micelles by Atomic Force Microscopy. *Pharmaceutical Research*. **1998**, 15, 1721-1726.

Liu Y.; Miyoshi H.; Nakamura M. Nanomedicine for Drug Delivery and Imaging: A Promising Avenue for Cancer Therapy and Diagnosis Using Targeted Functional Nanoparticles. *International Journal of Cancer*. **2007**, 120, 2527-2537.

Liu, R.; Li, D.; He, B.; Xu, X.; Sheng, M.; Lai, Y.; Wang, G.; Gu, Z. Anti-Tumor Drug Delivery of pH-Sensitive Poly(ethylene glycol)-Poly(L-histidine-)-Poly(L-lactide) Nanoparticles. *Journal of Controlled Release*. **2011**, 152, 49-56.

Liu, D.; Yang, F.; Xiong, F.; Gu, N. The Smart Drug Delivery System and Its Clinical Potential. *Theranostics*. **2016**, 6(9), 1306-1323.

Lund, R.; Willner, L.; Richter, D. Kinetics of Block Copolymer Micelles Studied by Small-Angle Scattering Methods. *Controlled Polymerization and Polymeric Structures, Springer*. **2013**, 51-158.

Maeda, H. The Enhanced Permeability and Retention (EPR) Effect in Tumor Vasculature: The Key Role of Tumor- Selective Macromolecular Drug Targeting. *Advances in Enzyme Regulation*. **2001**, 41, 189-207.

Maeda, H.; Bharate, G.; Daruwalla, J. Polymeric drugs for efficient tumor-targeted drug delivery based on EPR-effect. *European Journal of Pharmaceutics and Biopharmaceutics*. **2009**, 71, 409-419.

Maeda, H. Vascular Permeability in Cancer and Infection as Related to Macromolecular Drug Delivery, with Emphasis on the EPR Effect for Tumor-Selective Drug Targeting. *Proceedings of the Japan Academy*. **2012**, 88(3), 53-71.

Nomura, T.; Katunuma, N. Involvement of Cathepsins in the Invasion, Metastasis and Proliferation of Cancer Cells. *The Journal of Medical Investigation*. **2005**, 52, 1-9.

Oliveira, P.A.; Colaço, A.; Chaves R.; Guedespinto, H.; Delacruz, L.F.; Lopes, C. Chemical Carcinogenesis. *Anais da Academia Brasileira de Ciencias*. **2007**, 79(4), 593-616.

Ottevanger, P.; De Mulder, P. The quality of chemotherapy and its quality assurance. *European Journal of Surgical Oncology (EJSO).* **2005**, 31, 656-666.

Ozben, T. Mechanisms and Strategies to Overcome Multiple Drug Resistance in Cancer. *FEBS Letters*, **2006**. 580, 2903-2909.

Patel, N. R.; Pattni, B. S.; Abouzeid, A. H.; Torchilin, V. P. Nanopreparations to Overcome Multidrug Resistance in Cancer. *Advanced Drug Delivery Reviews*, **2013**, 65, 1748-1762.

Persidis, A. Cancer Multidrug Resistance. *Nature Biotechnology*, **1999**, 17, 94-95.

Qin, S.Y.; Zhang, A.Q.; Cheng, S.X.; Rong, L.; Zhang, X.Z. Drug Self-Delivery Systems for Cancer Therapy. *Biomaterials*. **2016**, 112, 234-247.

Rajora, A. K.; Ravishankar, D.; Osborn, H. M.; Greco, F. Impact of the Enhanced Permeability and Retention (EPR) Effect and Cathepsins Levels on the Activity of Polymer-Drug Conjugates. *Polymers*, **2014**, 6, 2186-2220.

Saraswathy, M.; Gong, S. Different Strategies to Overcome Multidrug Resistance in Cancer. *Biotechnology Advances*, **2013**, 31, 1397-1407.

Schmid, B.; Chung, D.E.; Warnecke, A.; Fichtner, I.; Kratz, F. Albumin-Binding Prodrugs of Camptothenic and Doxorubicin with an Ala-Leu-Ala-Leu-Linker That Are Cleaved by Cathepsin B: Synthesis and Antitumor Efficacy. *Bioconjugate Chemistry*. **2007**, 18(3), 702-716.

Simon, S.M. Role of Organelle pH in Tumor Cell Biology and Drug Resistance. *Drug Discovery Today*. **1999**, 4(1), 32-38.

Studer, M.; Kroger, L.A.; Denardo, S.J.; Kukis, D.L.; Meares, C.F. Influence of a Peptide Linker on Biodistribution and Metabolism of Antibody-Conjugated Benzyl-EDTA. Comparison of Enzymatic Digestion in Vitro and in Vivo. *Bioconjugate Chemistry*. **1992**, 3(5), 424-429.

Suk, J.S.; Xu, Q.; Kim, N.; Hanes, J.; Ensign, L.M. PEGylation as a Strategy for Improving Nanoparticle-Based Drug and Gene Delivery. *Advanced Drug Delivery Reviews*. **2016**, 99, 28-51.

Sunderland C. J.; Steiert M.; Talmadge J. E.; Derfus A. M.; Barry S.E. Targeted Nanoparticles for Detecting and Treating Cancer. *Drug Development Research*. **2006**, 67, 70-93.

Tong, R.; Cheng, J. Anticancer Polymeric Nanomedicines. *Polymer Reviews*. **2007**, 47, 345-381.

Veronese, F.M.; Harris, J.M. Introduction and Overview of Peptide and Protein Pegylation. *Advanced Drug Delivery Reviews*. **2002**, 54(4), 453-456.

Veronese, F. M.; Pasut, G. PEGylation, successful approach to drug delivery. *Drug discovery today*. **2005**, 10, 1451-1458.

Veronese, F.M.; Schiavon, O.; Pasut, G.; Mendichi, R.; Andersson, L.; Tsirk, A.; Ford, J.; Wu, G.; Kneller, S.; Davis, J.; Duncan, R. PEG-Doxorubicin Conjugates: Influence of Polymer Structure on Drug Release, in Vitro Cytotoxicity, Biodistribution, and Antitumor Activity. *Bioconjugate Chemistry*. **2005**, 16(4), 775-784.

Verweij, J.; De Jonge, M. Achievements and future of chemotherapy. *European Journal of Cancer*. **2000**. 36, 1479-1487.

Wong, H. L.; Bendayan, R.; Rauth, A. M.; Li, Y.; Wu, X. Y. Chemotherapy with Anticancer Drugs Encapsulated in Solid Lipid Nanoparticles. *Advanced Drug Delivery Reviews*. **2007,** 59, 491-504.

Xu P.; Van Kirk E. A.; Murdoch W. J.; Zhan Y.; Isaak D. D., Radosz M.; and Shen Y. Anticancer Efficacies of Cisplatin-Releasing pH-Responsive Nanoparticles. *Biomacromolecules*. **2006**, 7, 829-835.

Yang, G.; Liu, J.; Wu, Y.; Feng, L.; Liu, Z. Near-Infrared-Light Responsive Nanoscale Drug Delivery Systems for Cancer Treatment. *Coordination Chemistry Reviews*. **2016**, 320, 100-117.

Yano, M.; Hirai, K.; Naito, Z.; Yokoyama, M.; Ishiwata, T.; Shiraki Y.; Inokuchi, M.; Asano, G. Expression of Cathepsin B and Cystatin C in Human Breast Cancer. *Surgery Today*. **2001**, 31, 385-389.

Yin, Q.; Shen, J.; Zhang, Z.; Yu, H.; Li, Y. Reversal of Multidrug Resistance by Stimuli-Responsive Drug Delivery Systems for Therapy of Tumor. *Advanced Drug Delivery Reviews*, **2013**, 65, 1699-1715.

Yuan, Y.; Cai, T.; Xia, X.; Zhang, R.; Chiba, P.; Cai, Y. Nanoparticle Delivery of Anticancer Drugs Overcomes Multidrug Resistance in Breast Cancer. **2016**, *Drug Delivery*, 23, 3350–3357.

APPENDIX A.

SUPPLEMENTARY FIGURES

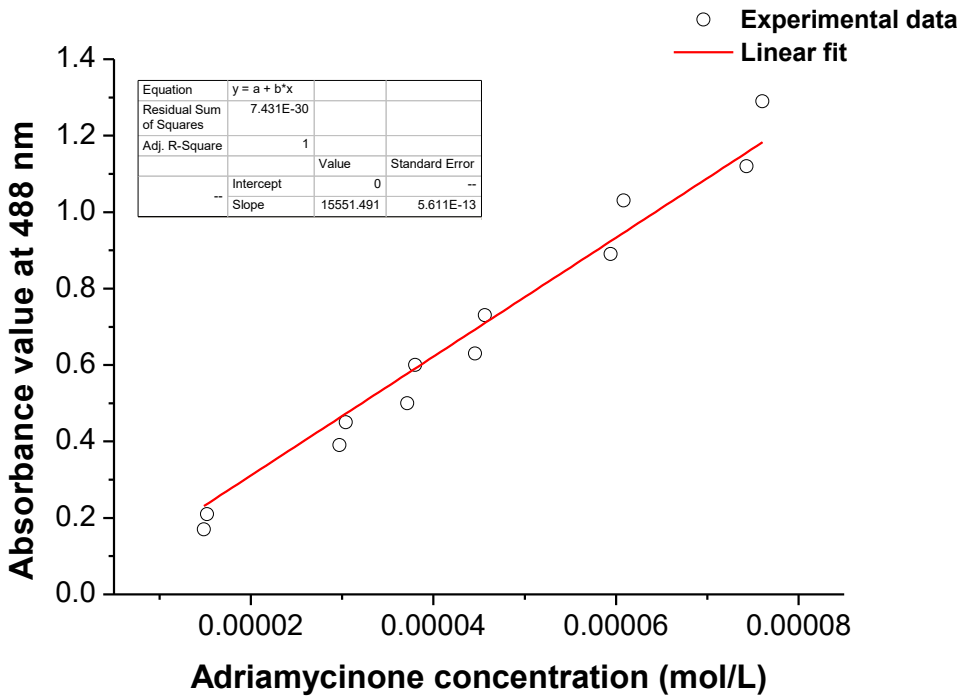

Figure A.1. The calibration curve of adriamycinone obtained at 488nm.

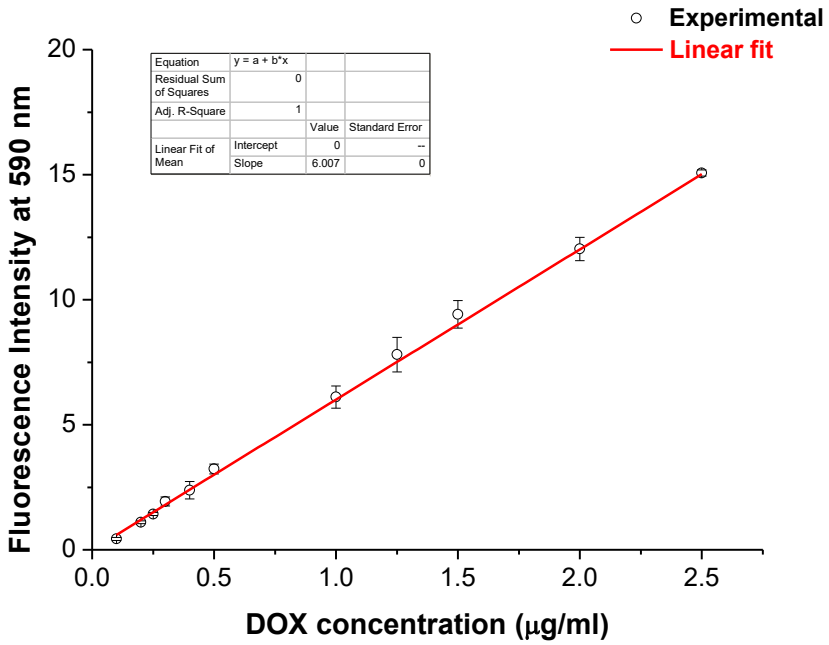

Figure A.2. The calibration curve of DOX using fluorescence intensity at 590 nm in PBS buffer at pH 7.4.

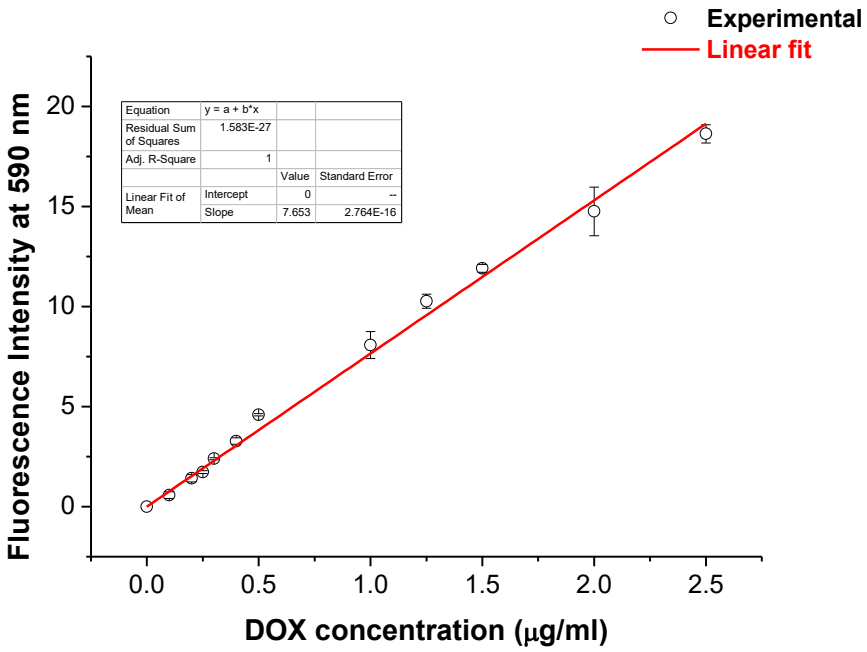

Figure A.3. The calibration curve of DOX using fluorescence intensity at 590 nm in acetate buffer at pH 5.0.

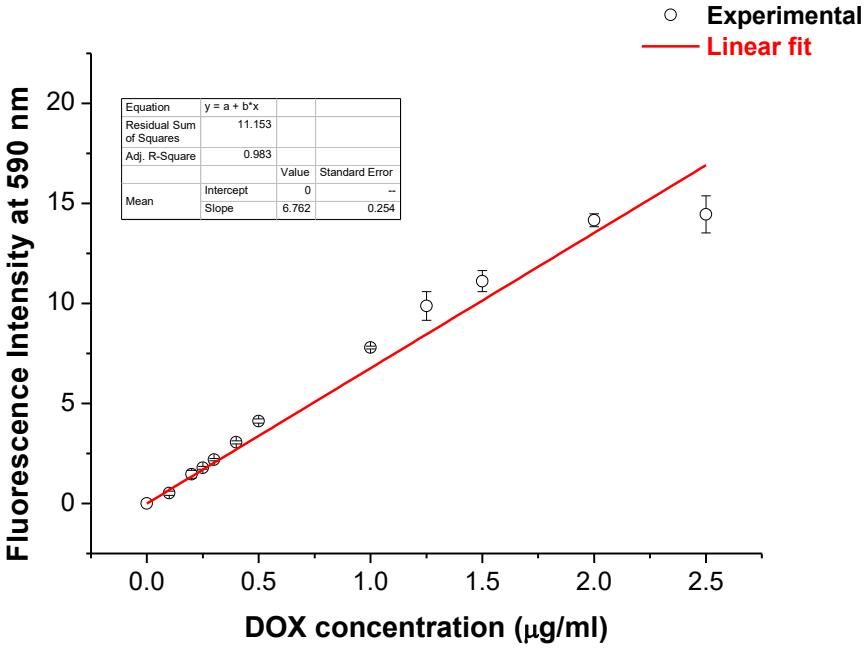

Figure A.4. The calibration curve of DOX using fluorescence intensity at 590 nm (prepared with 150 mM NaCl, 1 mM EDTA and 5mM L-cysteine in pH 5.0 acetate buffer).